A ratiometric, fluorescent BODIPY-based probe for transition and heavy metal ions

Wenwu Qin,[#,*] **Wei Dou,**[#] **Volker Leen,**[†] **Wim Dehaen,**[†] **Mark Van der Auweraer**[†] **and Noël Boens**[†,*]

[#] *Key Laboratory of Nonferrous Metal Chemistry and Resources Utilization of Gansu Province and State Key Laboratory of Applied Organic Chemistry, College of Chemistry and Chemical Engineering, Lanzhou University, Lanzhou 730000, China*
[†] *Department of Chemistry, KU Leuven (Katholieke Universiteit Leuven), Celestijnenlaan 200f, 3001 Leuven, Belgium*

Abstract

A novel metal ion-sensitive fluorescent probe − 4,4-difluoro-8-(4-methylphenyl)-5-(phenylethynyl)-3-[bis(pyridin-2-ylmethyl)amino]-4-bora-3a,4a-diaza-s-indacene − based on the BODIPY platform with di(2-picolyl)amine as chelator has been synthesized and spectroscopically and photophysically characterized. The generalized treatment of the solvent effect shows that solvent dipolarity is primarily responsible for the observed shifts of the absorption and fluorescence emission maxima. Complex formation with various metal ions is investigated in acetonitrile solution by means of spectrophotometric and fluorometric titrations. The BODIPY indicator forms 1:1 complexes with several transition metal (Ni^{2+}, Cu^{2+}, Zn^{2+}) and heavy metal (Cd^{2+}, Hg^{2+}) ions, producing large bathochromic shifts in the absorption and fluorescence spectra and, except for Ni^{2+}, cation-induced fluorescence amplifications. The dissociation constants of the metal ion complexes range from 4 μM for Hg^{2+} to 48 μM for Zn^{2+}.

---

[*] Corresponding authors: E-mail: qinww@lzu.edu.cn (W. Qin) and Noel.Boens@chem.kuleuven.be (N. Boens)

Introduction

Fluorescent probes for the measurement of concentrations of analytically and biologically important ions are essential tools in numerous fields of modern medicine and materials science.[1,2] The design and synthesis of fluorescent indicators with high selectivity and sensitivity for metal ions remain an exciting field of supramolecular chemistry. Of major importance are fluoroionophores targeting transition and heavy metal ions (such as Ni^{2+}, Cu^{2+}, Zn^{2+}, Cd^{2+}, Hg^{2+}, …). Ratiometric fluorescent probes which exhibit shifts in the absorption and/or fluorescence spectra upon coordination of the analyte of interest are preferred over probes with on/off switching of fluorescence. Indeed, measuring the ratio of the fluorescence signals at two suitably chosen wavelengths avoids the influence of many extraneous artifacts in fluorescence changes at a single wavelength. Therefore, the design, synthesis and spectroscopic characterization of ratiometric fluorescent chemosensors have emerged as an important area of supramolecular chemistry.

Here we describe a new ratiometric, fluorescent probe for transition and heavy metal ions based on the 4,4-difluoro-4-bora-3*a*,4*a*-diaza-*s*-indacene (BODIPY or *bo*ron *dipy*rrin or *bo*ron *dipy*rromethene)[3, 4] platform. Lately there is intense research interest in the synthesis and photophysical/spectroscopic properties of BODIPY-based fluorescent dyes and their application in selective and sensitive fluorescent chemosensors.[4c,4d] As a result, there are now thousands of different BODIPY dyes described in the literature with exciting structural variations. BODIPY is an outstanding fluorophore characterized by valuable properties including bright fluorescence [due to the combination of a high fluorescence quantum yield Φ with a large molar absorption coefficient $\varepsilon(\lambda)$] with absorption and fluorescence emission bands in the visible range, robustness towards chemicals and light, and generally a

negligible intersystem-crossing.[4] Moreover, the BODIPY core can be postfunctionalized easily (at the pyrrole carbons, the *meso*-carbon and the boron atom), leading to dyes with custom-made, fine-tuned spectroscopic properties for use in bioscience and material research.[5]

The transition and heavy metal ions of which the fluorometric/spectrophotometric detection is investigated are Cd^{2+}, Hg^{2+}, Ni^{2+}, Cu^{2+} and Zn^{2+}. As chelator for these ions, we chose bis(pyridin-2-ylmethyl)amine [commonly known as di(2-picolyl)amine, DPA], linked to the BODIPY core at the 3-position. Di(2-picolyl)amine is a chelator of several metal ions, including Mn^{2+}, Fe^{2+}, Co^{2+}, Ni^{2+}, Cu^{2+}, Zn^{2+}, Ag^+, Cd^{2+}, Hg^{2+} and Pb^{2+}.[6] Reported values of the dissociation constants K_d of the 1:1 complex $[Zn(DPA)]^{2+}$ are 158 nM [7] and 70 nM [8].

The literature of BODIPY-based fluorescent indicators, among them those for transition and heavy metal ions, has been reviewed recently by the KU Leuven authors.[4c] In addition, there are excellent reviews on fluorescent chemosensors for zinc ions based on different fluorophore platforms and various receptor units, including DPA and related *N,N*-bis(2-pyridylmethyl)ethane-1,2-diamine. [9] Of significant importance for this study are reports on fluoroionophores built on the BODIPY platform with DPA as ion receptor. A BODIPY-DPA Zn^{2+} probe with 30-fold fluorescence enhancement was reported by Nagano et al. (Chart 1). [10] A fluorescent sensor for Zn^{2+} ($K_d = 1$ nM), based on photoinduced electron transfer (PET), utilizing BODIPY linked at the *meso*-position to the DPA chelator (Chart 1), which displays a significant fluorescence enhancement upon Zn^{2+} binding, was described by Peng and coworkers.[11] The same research group also reported a selective sensor for imaging Cd^{2+} in living cells, using the BODIPY scaffold (K_d is ca. 60 μM), but with the DPA chelator attached at the 3-position through a *p*-styryl spacer (Chart

1).[12] A very similar BODIPY-styryl linked DPA chelator (Chart 1) was described by Akkaya and coworkers, but it was reported as being selective for Zn^{2+} (K_d = 20 µM), though Hg^{2+} and Cd^{2+} also showed some response.[13] Although the ratiometric probes of Peng[12] and Akkaya[13] are very alike (see Chart 1), they display a different selectivity (Cd^{2+} vs. Zn^{2+}). Usually discrimination between Cd^{2+} and Zn^{2+} is very difficult because they are stereoelectronic isosteres. For Ni^{2+} detection, only one account on a BODIPY-based fluorescent sensor can be found in the literature.[14] This fluorescence turn-on (PET) probe (K_d = 0.2 mM) shows a ca. 25-fold fluorescence increase upon Ni^{2+} binding with no shifts in absorption and emission maxima. Since paramagnetic Cu^{2+} is a notorious fluorescence quencher, few ratiometric fluorescent chemosensors for Cu^{2+} are available in the literature.[4c, 15] A colorimetric and near-IR fluorescent turn-on BODIPY-based probe with DPA as a chelator with high selectivity for Cu^{2+} among several transition metal ions has been reported by the KU Leuven authors (Chart 1).[16a] Similar BODIPY-DPA derived colorimetric and NIR fluorescent chemosensors for Cu^{2+} (Chart 1) have been described by Yin and coworkers.[16b, 16c] BODIPY-DPA functionalized hydroxyapatite (HA) nanoparticles formed 1:1 complexes with Cd^{2+} or Zn^{2+} with large cation-induced fluorescence amplifications,[17] whereas BODIPY-functionalized silica nanoparticles exhibited high specificity for Cu^{2+} over other transition metal ions in aqueous-organic media and resulted in notable fluorescence quenching, as reported by Qin et al.[18] Fluorescent probes for lead, cadmium and mercury[19] ions have been reviewed recently.[20]
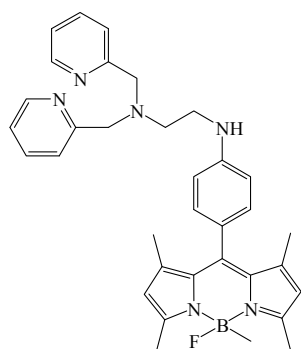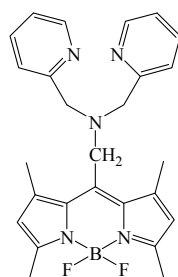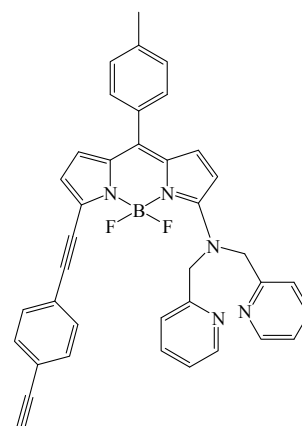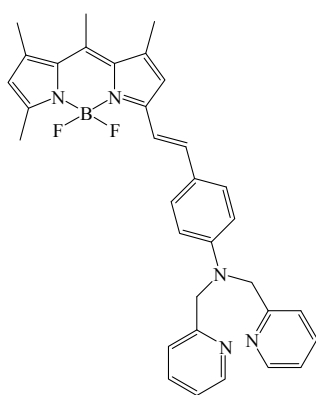
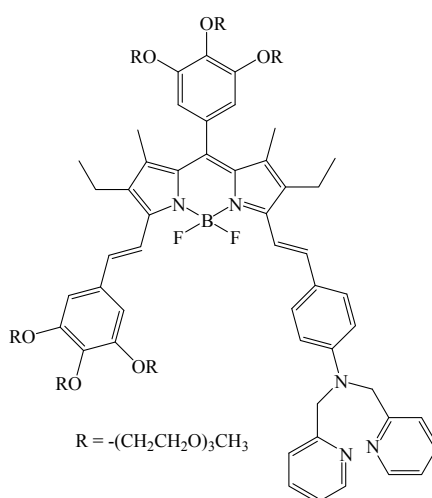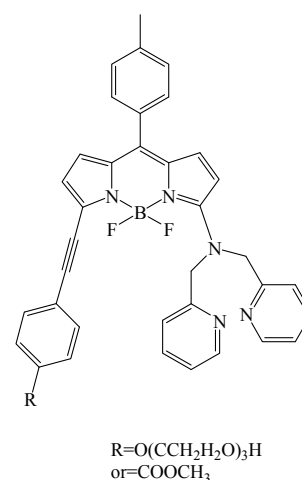**Chart 1.** BODIPY-DPA linked probes described in the literature.[10-13, 16]

In this work, we synthesized the chemosensor **1** with BODIPY as fluorophore coupled at the 3-position to the DPA chelator and to a phenylethynyl subunit at the 5-position. The phenylethynyl moiety at 5-position causes a red shift of the spectra in relation to unsubstituted and common BODIPY dyes.[5, 21] The solvent-dependent spectroscopic/photophysical characteristics of **1** were investigated by steady-state UV−vis spectrophotometry and fluorometry. Coordination of **1** to various metal ions (Na$^+$, K$^+$, Mg^{2+}, Ca^{2+}, Ni^{2+}, Cu^{2+}, Zn^{2+}, Cd^{2+}, Hg^{2+}) was spectroscopically studied and discussed. The measured ground-state dissociation constants K_d for the formed complexes, the absorption and fluorescence emission maximal wavelengths in the

absence and presence of ions, the fluorescence quantum yields Φ of the apo and ion-bound species of **1** are presented and discussed.

Results and Discussion

Synthesis

Fluorescent probe 4,4-difluoro-8-(4-methylphenyl)-5-(phenylethynyl)-3-[bis(pyridin-2-ylmethyl)amino]-4-bora-3*a*,4*a*-diaza-*s*-indacene (**1**) was synthesized by nucleophilic substitution of 3-chloro-4,4-difluoro-8-(4-methylphenyl)-5-(phenylethynyl)-4-bora-3*a*,4*a*-diaza-*s*-indacene (**2**) with bis(pyridin-2-ylmethyl)amine (DPA, **3**) (Scheme 1). Compound **2** was synthesized according to our published procedure.[22]
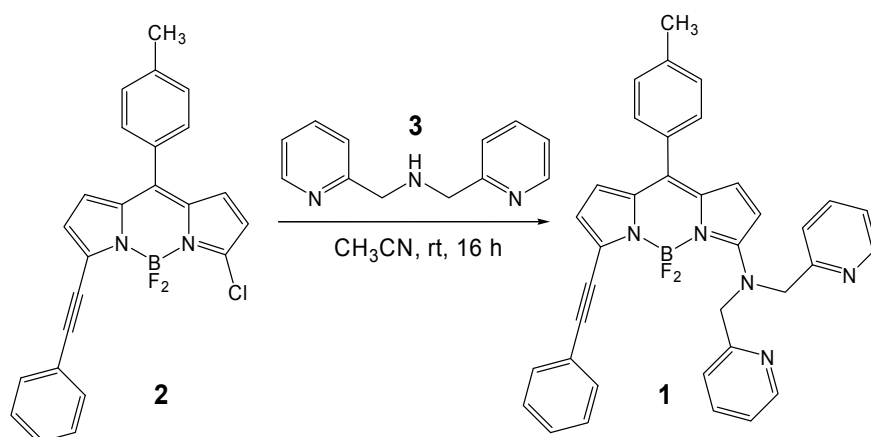
Scheme 1. Synthesis of compound **1**.

UV–vis spectroscopy

A selection of UV–vis absorption and fluorescence emission spectra of **1** dissolved in a series of solvents is depicted in Figure 1. The spectroscopic/photophysical properties of **1** are compiled in Table 1. The maximum of the main absorption band [λ_{abs}(max)] of **1**, attributed to the 0−0 vibrational band of a strong $S_1 \leftarrow S_0$ transition, is located between 525 nm (in acetonitrile) and 561 nm (in cyclohexane), corresponding to a energy difference of ca. 1200 cm^{-1}. A shoulder in the 510–525 nm range at the

short wavelength side of the spectrum is assigned to the 0−1 vibrational band of the same transition. This vibrational fine structure is undetectable in the more polar solvents (i.e. DMSO, acetonitrile, DMF and methanol, see Figure 1a). The typical, narrow BODIPY-like main absorption band is not observed for **1**. The most narrow absorption bands are detected in cyclohexane, toluene, dibutyl ether, pentan-1-ol and octan-1-ol. The full width at half height of the maximum of the absorption band (fwhm$_{abs}$) increases from ca. 2700 cm^{-1} in cyclohexane to ca. 3900 cm^{-1} in butanenitrile. The broadening of the absorption spectra in the more polar solvents indicates a change in the size or orientation of the permanent dipole moment upon excitation, which could correspond to a partial charge-transfer character for the lowest excited state in the ground-state geometry. To make this observation compatible with the blue shift of the absorption spectra upon increasing solvent dipolarity, one has to assume that the size of the permanent dipole moment probably decreases upon excitation or that excitation changes rather the orientation than the size of the permanent dipole moment. A closer inspection of the data in Table 1 suggests that a red shift related to an increased solvent polarizability and the resulting increased dispersion and Van der Waals interactions is accompanied by a blue shift upon increasing the dipolarity of the solvent.

The structureless fluorescence emission of **1** also is solvent dependent (Figure 1b). The maximum of the structureless emission, λ_{em}(max), shifts from 575 nm in acetonitrile to 594 nm in toluene. This red shift (ca. 560 cm^{-1}) is accompanied by a decrease of the emission bandwidth fwhm$_{em}$ (from ca. 1700 cm^{-1} in acetonitrile to ca. 1300 cm^{-1} in toluene). This suggests an increase of the permanent dipole moment or a change of the orientation of the permanent dipole moment during the return to the Franck-Condon ground state.
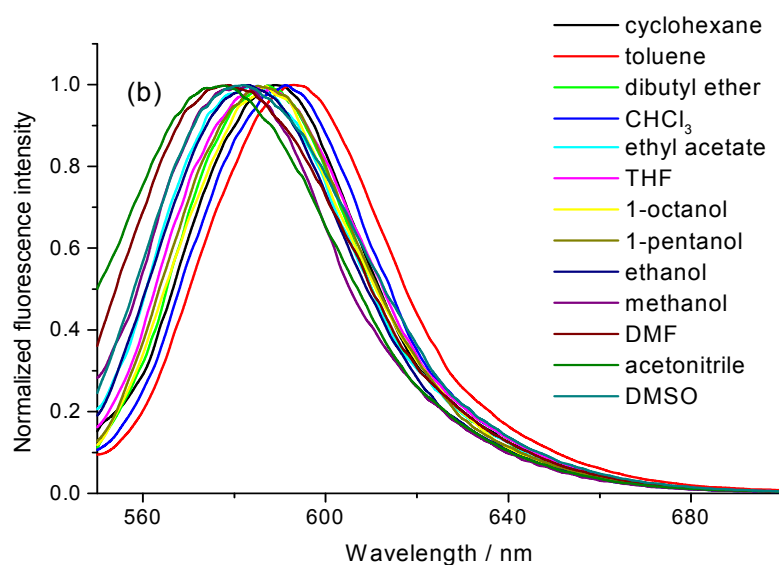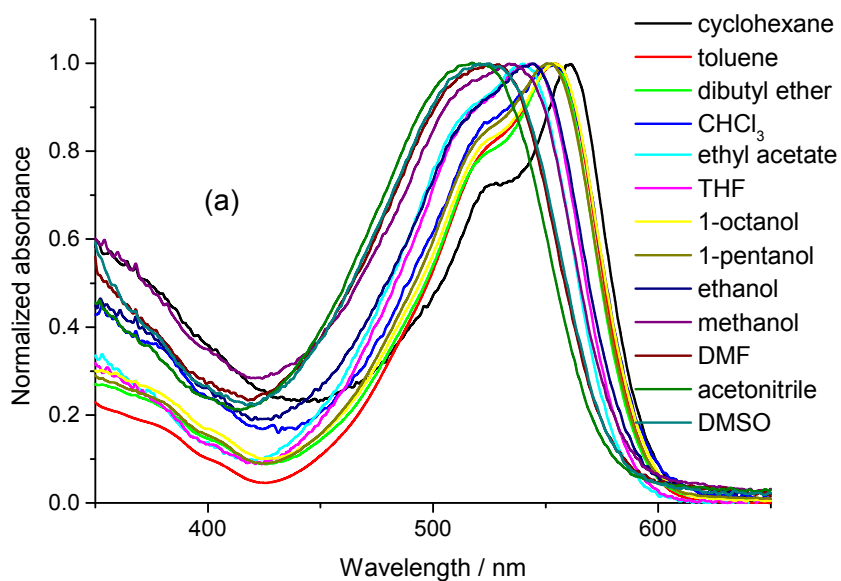
Figure 1. (a) Normalized absorption spectra of **1** in a selection of solvents. (b) Corresponding normalized fluorescence emission spectra (excitation at 530 nm, except for acetonitrile, DMF and DMSO with excitation at 510 nm).

Table 1. Spectroscopic and photophysical properties of **1** in several solvents.

#[a]	Solvent	λ_{abs}(max) [nm]	λ_{em}(max) [nm]	λ_{ex}(max) [nm]	$\Delta \bar{\nu}$ [cm^{-1}]	fwhm$_{abs}$ [cm^{-1}]	fwhm$_{em}$ [cm^{-1}]	Φ [b]
1	Cyclohexane	561	589	561	847	2720	1300	0.18 ± 0.03
2	Toluene	554	594	555	1216	2720	1340	0.180 ± 0.002
3	Dibutyl ether	553	587	556	1047	2770	1310	0.134 ± 0.005
4	Diethyl ether	550	590	552	1233	3000	1390	0.106 ± 0.002

5	Chloroform	552	590	553	1167	3450	1320	0.24 ± 0.03
6	Ethyl acetate	539	584	543	1430	3180	1450	0.12 ± 0.01
7	THF [c]	542	585	545	1356	3100	1430	0.156 ± 0.006
8	1-Octanol	554	587	554	1015	2910	1330	0.497 ± 0.004
9	1-Pentanol	552	586	552	1051	2930	1390	0.30 ± 0.01
10	1-Butanol	550	586	552	1117	3040	1530	0.38 ± 0.01
11	2-Propanol	548	586	550	1183	2980	1390	0.313 ± 0.006
12	Acetone	530	582	534	1686	3490	1750	0.103 ± 0.008
13	Butanenitrile	529	582	532	1721	3900	1580	0.131 ± 0.006
14	Ethanol	542	583	543	1298	3220	1410	0.165 ± 0.008
15	Methanol	538	582	541	1405	3760	1360	0.115 ± 0.004
16	DMF [c]	527	577	530	1644	3620	1660	0.158 ± 0.001
17	Acetonitrile	525	575	527	1656	3670	1710	0.108 ± 0.006
18	DMSO [c]	526	581	530	1800	3660	1580	0.26 ± 0.02

[a] The solvents are numbered according to increasing dielectric constant. [b] Φ values were determined vs. cresyl violet as reference ($\Phi_{\square}$ = 0.55). Excitation wavelength λ_{ex} was 530 nm, except for DMF, acetonitrile and DMSO with λ_{ex} = 510 nm. [c] THF = tetrahydrofuran, DMF = N,N-dimethylformamide, DMSO = dimethyl sulfoxide.

It is useful to determine the origin of the solvent-dependent spectral changes because these deliver information on the nature of the ground and excited states. The most recent, comprehensive treatment of the solvent effect (based on a set of four empirical, complementary, mutually independent solvent scales, i.e., dipolarity, polarizability, acidity and basicity of the medium) has been proposed by Catalán.[23] In this method, the polarizability and dipolarity of a particular solvent are characterized by the parameters SP and SdP, respectively, whereas acidity and basicity are described by the scales SA and SB, respectively. The {SA, SB, SP, SdP} parameters for a large number of solvents can be found in ref 23. Mathematically, the solvent effect on the physicochemical observable y can be expressed by the multilinear eqn 1:

$$y = y_0 + a_{SA}\,SA + b_{SB}\,SB + c_{SP}\,SP + d_{SdP}\,SdP \tag{1}$$

where y_0 denotes the physicochemical property of interest in the gas phase; a_{SA}, b_{SB}, c_{SP} and d_{SdP} are regression coefficients that describe the sensitivity of the property y to

the various solvent–solute interaction mechanisms; {SA, SB, SP, SdP} are independent solvent parameters (indices) accounting for the various types of solvent–solute interactions.

The spectroscopic observables y analyzed in this paper are the absorption maxima $\bar{\nu}_{abs}$ [= $1/\lambda_{abs}$(max)] and the fluorescence emission maxima $\bar{\nu}_{em}$ [= $1/\lambda_{em}$(max)], both expressed in cm^{-1}. The use of {SA, SB, SP, SdP} (eqn 1) gives high-quality fits of $\bar{\nu}_{abs}$ of **1** (for the solvents listed in Table 1), using the correlation coefficient r as goodness-of-fit criterion (r = 0.939, eqn 2a and Electronic Supplementary Information, ESI). Good-quality fits are also obtained for the multilinear analysis of $\bar{\nu}_{em}$ according to eqn 1 (r = 0.827, eqn 2b and ESI). The extra benefit of the generalized (Catalán) treatment of the solvent effect is that it allows one to separate the relative contributions of dipolarity, polarizability, acidity and basicity of the medium. Therefore, we utilized the new methodology to resolve which solvent property/properties is/are responsible for the observed shifts of $\bar{\nu}_{abs}$ and $\bar{\nu}_{em}$. The relative importance of each of the Catalán solvent scales was studied by omitting in turn one, two or three solvent scales from the regression analysis (for details, see ESI). These analyses clearly identify solvent dipolarity (SdP) as the most critical parameter that accounts for the observed shifts of $\bar{\nu}_{abs}$ and $\bar{\nu}_{em}$. Moreover, only for SdP are the estimated d_{SdP} coefficients significantly larger than their associated standard errors.

$$\bar{\nu}_{abs} = (18.2\pm0.5)\times10^3 + (-841\pm249)\,SA + (-54\pm170)\,SB + (-625\pm649)\,SP + (1.3\pm0.1)\times10^3\,SdP \quad (2a)$$

$$\bar{\nu}_{em} = (17.2\pm0.3)\times10^3 + (-178\pm142)\,SA + (31\pm97)\,SB + (-474\pm371)\,SP + (3.9\pm0.8)\times10^2\,SdP \quad (2b)$$

**Complex formation between 1 and various metal ions in acetonitrile**

To investigate the chelating ability of **1**, UV–vis spectrophotometric and fluorometric titrations were carried out in acetonitrile solution as a function of metal ion concentration. Complex formation was examined for **1** with alkali (Na^+ and K^+),

alkaline-earth (Mg^{2+} and Ca^{2+}), transition metal (Ni^{2+}, Cu^{2+}, Zn^{2+}) and heavy metal (Cd^{2+} and Hg^{2+}) ions. The results are summarized in Table 2.

Upon addition of the alkali ions Na^+ and K^+ and the alkaline-earth ions Mg^{2+} and Ca^{2+} to a solution of **1** in acetonitrile, no change in the UV–vis absorption and fluorescence spectra could be detected. Obviously, the interaction between **1** and these ions is too weak to cause any change of either the UV–vis absorption spectra or the vis fluorescence spectra.

Conversely, the transition metal (Ni^{2+}, Cu^{2+}, Zn^{2+}) and heavy metal (Cd^{2+}, Hg^{2+}) ions produced spectral changes of **1** (Figure 2). For example, the lowest-energy absorption band of **1** shifts bathochromically by ca. 40 nm, from 525 nm in an ion-free environment to 565 nm upon addition of Zn^{2+} to the acetonitrile solution (Figure 3a). The relative contributions of the 565/525 nm signals change with varying [Zn^{2+}] and the vis absorption spectra show isosbestic points at 434 and 540 nm. Similar changes were observed in the fluorescence excitation spectra (Figure S1, ESI). The maximum of the fluorescence emission band shifts bathochromically from 575 nm in ion-free acetonitrile to 584 nm in the presence of Zn^{2+} and is accompanied by an increase in intensity (Figure 3b). A pseudo-isoemissive point can be observed at 564 nm, which can be used to simplify analysis of ratiometric fluorometric titrations. The fluorescence quantum yield Φ of **1** increases from 0.11 in the absence of Zn^{2+} to 0.29 for the **1**–Zn^{2+} complex. These red shifts can be rationalized as follows. Upon complexation of Zn^{2+}, the lone pair of N of DPA connected to C3 of BODIPY will become less available for delocalization over the BODIPY moiety. One should note also that, upon complexation of Zn^{2+}, the features of the absorption spectra become closer to that of unsubstituted and common BODIPYs showing a narrow band and a hint of vibrational fine structure even in polar solvents.[5,24] This can be attributed again

to the blocking of the delocalization of the lone pair of N of DPA in 3-position over the rest of the conjugated system. The same effect will decrease the dipole moments (and their differences between ground and excited state) in the ground and excited state. This also accounts for the strong decrease of the Stokes shift from 1660 cm^{-1} in **1** to 580 cm^{-1} in **1**–Zn^{2+} and of both fwhm$_{abs}$ and fwhm$_{em}$ of **1**–Zn^{2+} (Table 2). Often BODIPYs with explicit electron-withdrawing or electron-donating substituents are characterized by low Φ values, especially in polar solvents.[25] Upon complexation by Zn^{2+}, the electron-donating effect of N in 3-position is significantly decreased which leads to an increase of Φ from 0.11 to 0.29.

12
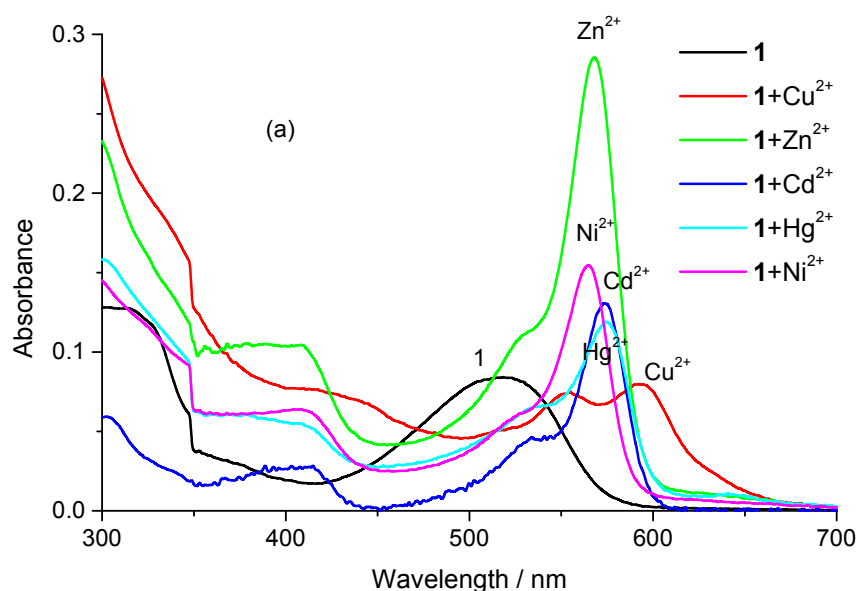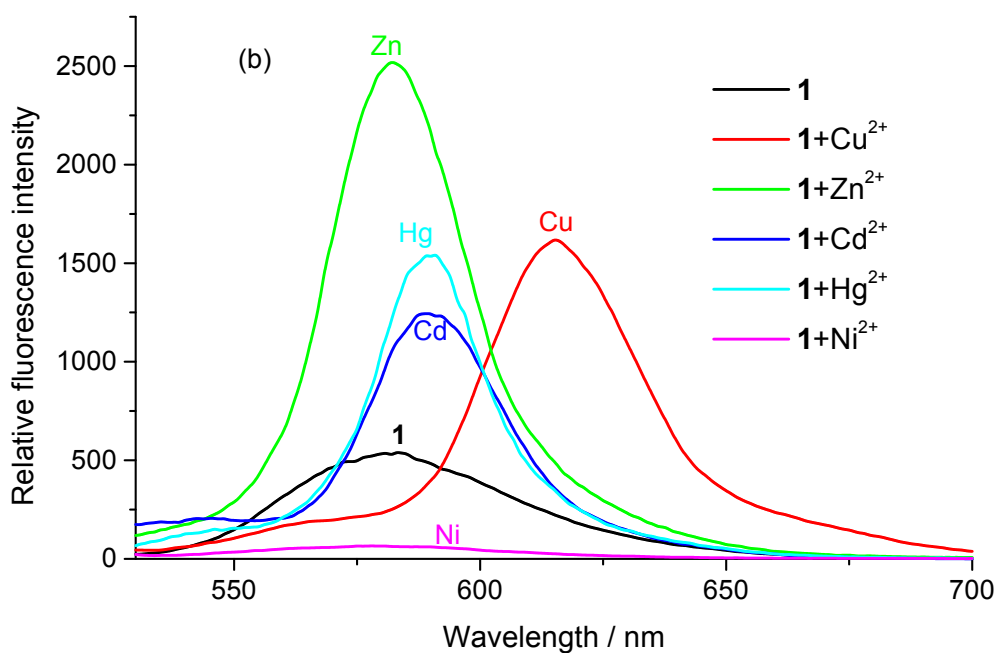
Figure 2. (a) Absorption and (b) fluorescence emission spectra of apo **1** and of **1** in the presence of the transition metal ions Cu^{2+} (60 μM), Zn^{2+} (600 μM), Ni^{2+} (170 μM) and the heavy metal ions Cd^{2+} (235 μM) and Hg^{2+} (50 μM) in acetonitrile.

Analysis of the UV-vis spectrophotometric and vis fluorometric titration data in the presence of varying concentrations of Zn^{2+} allows one to extract the ground-state dissociation constant K_d and the stoichiometry of the **1**–Zn^{2+} complex. The values of K_d and the stoichiometry (n) of binding of Zn^{2+} by the DPA ligand of **1** were determined by nonlinear fitting eqn 3 (direct fluorometric titration)[26] and eqn 4 (ratiometric fluorometric titration)[26] to the fluorescence excitation or emission spectral data F (eqn 3) and ratios R (eqn 4), measured as a function of metal ion concentration, i.e., $[X] = [Zn^{2+}]$. Nonlinear least-squares analyses of the corresponding spectrophotometric titrations (direct and ratiometric) as a function of metal ion were also performed.[27] In all titrations, no metal ion buffer was used to control the free metal ion concentration. It was assumed that the free metal ion concentration $[X]$ could be approximated by its analytical concentration.

13

$$F = \frac{F_{\max}[\text{X}]^n + F_{\min}K_d}{K_d + [\text{X}]^n} \qquad (3)$$

In eqn 3, F stands for the fluorescence signal at free ion concentration [X], whereas $F_{\min}$ and $F_{\max}$ denote the fluorescence signals at minimal and maximal [X], respectively, and n is the number of cations bound per probe molecule (i.e., stoichiometry of binding). Because the fits of eqn 3 to the fluorescence data F with n, K_d, $F_{\min}$ and $F_{\max}$ as freely adjustable parameters always gave values of n close to 1 (indicative of a 1:1 complex), $n = 1$ was used in the final curve fittings, from which the estimated K_d values are reported here. The plot of F against $-\log$ [X] has a sigmoidal shape. This plot starts at $F_{\min}$ at very low [X] and changes most in the X-concentration range from $0.1 \times K_d$ to $10 \times K_d$ to asymptotically reach $F_{\max}$ at high [X]. Outside this critical X-concentration range, F does not change much. Therefore, it important that the dissociation constant K_d is well matched with the X-concentration range of interest.

$$R = \frac{R_{\max}[\text{X}]^n + R_{\min}K_d\xi}{K_d\xi + [\text{X}]^n} \qquad (4)$$

In the *excitation* ratiometric method, one measures $R = F\left(\lambda_{\text{em}}, \lambda_{\text{ex}}^1\right) \big/ F\left(\lambda_{\text{em}}, \lambda_{\text{ex}}^2\right)$ at a common emission wavelength, λ_{em}, and two different excitation wavelengths, λ_{ex}^1 and λ_{ex}^2. $R_{\min}$ is the ratio of the fluorescence intensities at two distinct excitation wavelengths and one emission wavelength of the apo form of the indicator (minimum [X]). $R_{\max}$ represents the ratio of the fluorescence intensities of the bound form of the indicator (maximum [X]). R denotes the ratio of the fluorescence intensities corresponding to intermediate [X] and $\xi = F_{\min}\left(\lambda_{\text{em}}, \lambda_{\text{ex}}^2\right) \big/ F_{\max}\left(\lambda_{\text{em}}, \lambda_{\text{ex}}^2\right)$. Choosing the wavelength of the pseudo-isoemissive point as λ_{ex}^2 makes the analysis simpler. In this

case we have $\xi = 1$ and the expression for R (eqn 4) simplifies to that of F (eqn 3). Fitting eqn 4 to *excitation* ratiometric values R as a function of [X] yields values for $K_d \xi\left(\lambda_{em}, \lambda_{ex}^2\right)$, R_{min}, R_{max} and n. Because $\xi\left(\lambda_{em}, \lambda_{ex}^2\right)$ – the ratio of the fluorescence signal of the apo form of the indicator over that of the bound form at the indicated wavelengths – is experimentally accessible, a value for K_d can be recovered from ratiometric excitation fluorescence data.

In the *emission* ratiometric method, one determines $R = F\left(\lambda_{em}^1, \lambda_{ex}\right)/F\left(\lambda_{em}^2, \lambda_{ex}\right)$ at the indicated wavelengths as a function of cation concentration [X]. In this case, ξ is defined as $\xi = F_{min}\left(\lambda_{em}^2, \lambda_{ex}\right)/F_{max}\left(\lambda_{em}^2, \lambda_{ex}\right)$. $\xi = 1$ when λ_{ex}^2 is chosen as the wavelength corresponding to the pseudo-isoemissive point and, in that case, the expression for R (eqn 4) simplifies to that of F (eqn 3). Fitting eqn 4 to the *emission* ratiometric fluorescence data R as a function of [X] yields values for $K_d \xi\left(\lambda_{em}^2, \lambda_{ex}\right)$, R_{min}, R_{max} and n. Because $\xi\left(\lambda_{em}^2, \lambda_{ex}\right)$ can be determined from the fluorescence signals of the apo and bound forms of the indicator at the indicated wavelengths, a value K_d for the complex can be obtained.

Table 2. Spectroscopic and photophysical characteristics of **1** in the absence and presence of transition metal (Ni^{2+}, Cu^{2+}, Zn^{2+}) and heavy metal (Cd^{2+}, Hg^{2+}) ions in acetonitrile. K_d is the average value determined from all the (direct and ratiometric) analyses of fluorometric and spectrophotometric titrations.

Complex	$\lambda_{abs}(max)$ [nm]	$\lambda_{em}(max)$ [nm]	Isosbestic points [nm]	$\Delta\overline{V}$ [cm^{-1}]	K_d [µM]	fwhm$_{abs}$ [cm^{-1}]	fwhm$_{em}$ [cm^{-1}]	Φ
1	525	575		1656		3670	1710	0.108±0.006
1−Ni^{2+}	565	580	540, 443	458	13 ± 2	1120	1800	0.020±0.004
1−Cu^{2+}	594	616	547, 463	601	9 ± 3	−	950	0.40 ± 0.03
1−Zn^{2+}	565	584	540, 434	576	48 ± 11	1100	900	0.29 ± 0.05
1−Cd^{2+}	575	590	540, 438	442	9 ± 2	950	920	0.23 ± 0.02
1−Hg^{2+}	575	590	537, 438	442	4 ± 1	2000	840	0.27 ± 0.02

From the analyses of all the direct and ratiometric spectrophotometric and fluorometric titrations of **1** with Zn^{2+} ions it is clear that a 1:1 ligand/cation stoichiometry is found with an average K_d value for the **1**–Zn^{2+} complex of 48 ± 11 µM.
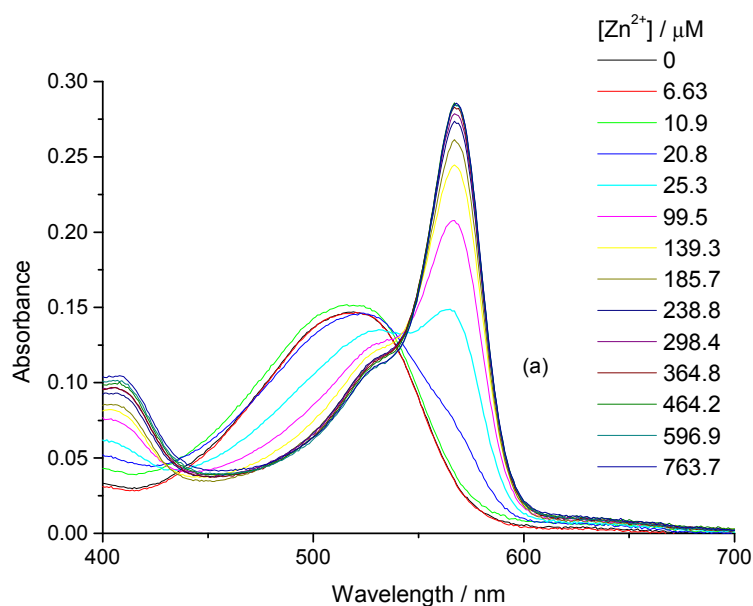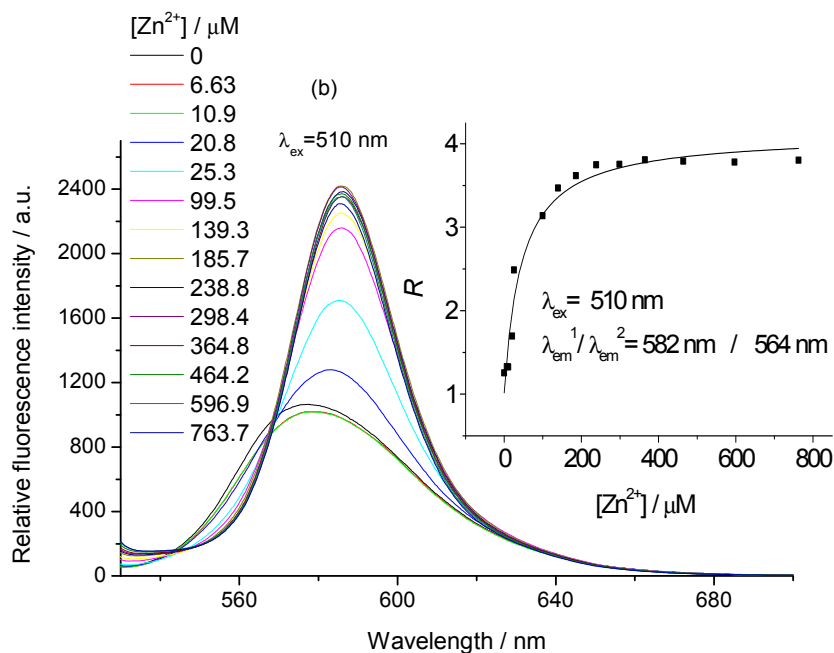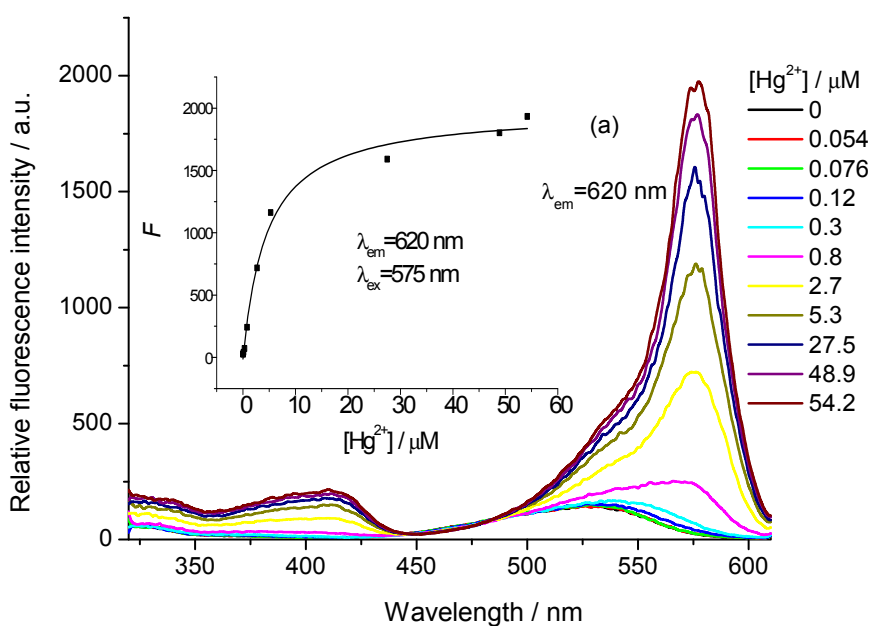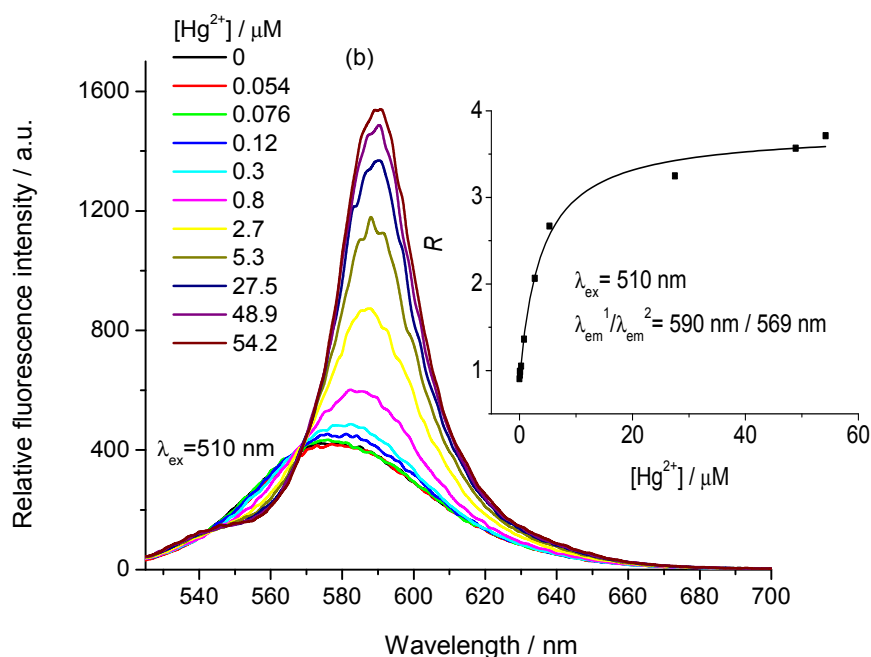
Figure 3. Compound **1** as a function of $[Zn^{2+}]$ in acetonitrile solution. (a) Absorption spectra. (b) Fluorescence emission spectra (excitation at 510 nm). The full line in the inset shows the best fit to the ratiometric emission (eqn 4 with n = 1) titration data at $\lambda_{em}^1 / \lambda_{em}^2$ = 582 nm / 564 nm (isoemissive point) as a function of $[Zn^{2+}]$.

The vis absorption and fluorescence (excitation/emission) spectral changes observed when Cd^{2+} is added to **1** in acetonitrile solution are comparable to those for Zn^{2+} (Figure S2, ESI), although the bathochromic shifts upon complex formation are somewhat larger $[\lambda_{abs}(max) = 575$ nm, $\lambda_{em}(max) = 590$ nm$]$ and Φ of the **1**–Cd^{2+} complex is slightly lower than that of **1**–Zn^{2+} (Table 2). In the emission spectra as a function of $[Cd^{2+}]$ pseudo-isoemissive points can be found at 571 and 550 nm. An average K_d value of 9 ± 2 μM was obtained for the **1**–Cd^{2+} complex. This smaller K_d value (compared to K_d of the **1**–Zn^{2+} complex) suggests a stronger bond between Cd^{2+} and the N ligands of DPA. Hence, the lone pair of N connected to C3 of the BODIPY framework will be less available for delocalization over the conjugated system, leading to somewhat larger red spectral shifts than those observed for Zn^{2+}.

The response of the absorption and fluorescence (excitation/emission) spectra of **1** in acetonitrile upon addition of Hg^{2+} (Figure 4) is nearly the same as that found for **1** in the presence of Cd^{2+}, but Φ of **1**–Hg^{2+} is somewhat higher than Φ of **1**–Cd^{2+} (Table 2). This Φ value is unexpected taking into account the possible heavy-atom quenching by Hg^{2+}. The emission spectra as a function of $[Hg^{2+}]$ show two pseudo-isoemissive points, at 569 and 544 nm. The average K_d value of the **1**−Hg^{2+} complex was found to be 4 ± 1 µM.

Figure 4. Compound **1** in acetonitrile solution as a function of [Hg^{2+}]. (a) Fluorescence excitation spectra (emission observed at 620 nm). (b) Fluorescence emission spectra (excitation at 510 nm). The full line in the insets of (a) and (b) shows the best fit to (a) the direct fluorometric excitation (eqn 3 with $n = 1$) titration data at $\lambda_{ex} = 575$ nm, $\lambda_{em} = 620$ nm and (b) the ratiometric emission (eqn 4 with $n = 1$) at $\lambda_{em}^1/\lambda_{em}^2 = 590$ nm/569 nm (isoemissive point) titration data as a function of [Hg^{2+}].

Upon addition of Ni^{2+} to a solution of **1** in acetonitrile, the vis absorption spectra respond analogously to the addition of Zn^{2+}: a ca. 40 nm red shift (to 565 nm) is found in addition to the appearance of isosbestic points at 443 and 540 nm. In contrast, addition of Ni^{2+} causes strong fluorescence quenching: Φ of **1**–Ni^{2+} is only 0.02 compared to 0.11 for apo **1**. Quenching of fluorescence upon Ni^{2+} binding arises from a PET from the BODIPY fluorophore to the metal center. Ni^{2+} has – in contrast to the close-shell ions Zn^{2+}, Cd^{2+} and Hg^{2+} – several low-lying *dd*-type excited states and is moreover paramagnetic. The influence of Ni^{2+} on the spectral maxima and the features of the absorption and emission spectra can be clarified in the same way as for Zn^{2+}, Cd^{2+} and Hg^{2+}. The absorption and fluorescence emission spectra of **1** in acetonitrile as a function of [Ni^{2+}] are given in Figure S3 (ESI). The average K_d value of the **1**−Ni^{2+} complex amounted to 13 ± 2 μM.
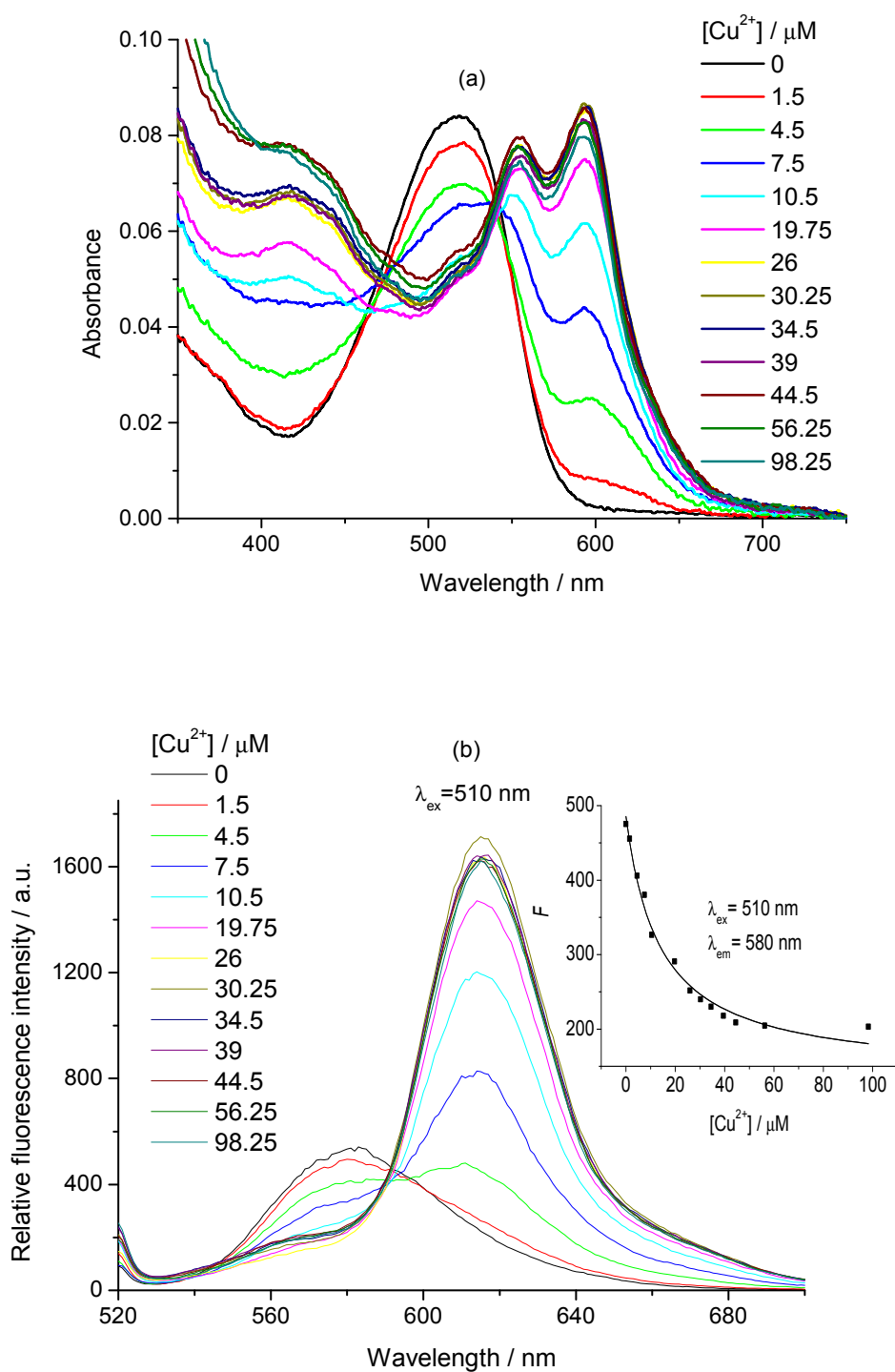
Figure 5. Compound **1** in acetonitrile solution as a function of $[Cu^{2+}]$. (a) Absorption spectra. (b) Fluorescence emission spectra (excitation at 510 nm). The full line in the inset of (b) shows the best fit to the direct fluorometric emission titration data (eqn 3 with $n = 1$) at $\lambda_{em} = 580$ nm as a function of $[Cu^{2+}]$.

Compared to the transition and heavy metal ions Ni^{2+}, Zn^{2+}, Cd^{2+} and Hg^{2+}, addition of Cu^{2+} triggers a large fluorescence enhancement ($\Phi = 0.40$ for **1**–Cu^{2+}) and

the largest red shifts [λ_{abs}(max) = 594 nm, λ_{em}(max) = 616 nm] (Figure 2 and Figure 5). The average K_d value of $\mathbf{1}-Cu^{2+}$ complex was 9 ± 3 μM. The Stokes shift of the $\mathbf{1}-Cu^{2+}$ complex (600 cm^{-1}) is larger than those of the $\mathbf{1}-Cd^{2+}$ and $\mathbf{1}-Hg^{2+}$ complexes (440 cm^{-1}) and close to that of the $\mathbf{1}-Zn^{2+}$-complex (580 cm^{-1}). Also the large increase in Φ is quite unexpected because Cu^{2+} is paramagnetic and has low-lying dd-states. Both properties are analogous to Ni^{2+}, which strongly quenches the BODIPY fluorescence. Although the absorption spectrum of $\mathbf{1}$ undergoes a red shift upon complex formation with Cu^{2+} (in analogy to what occurs upon complex formation with the other divalent ions), the features of the absorption spectrum of the $\mathbf{1}-Cu^{2+}$ complex differ in several aspects from those of the other complexes. First, the apparent ratio of the 0–1 to the 0–0 band of the $S_1 \leftarrow S_0$ transition decreases from 0.9 for Cu^{2+} to 0.3–0.4 for the other ions. Second, the ratio of the maximum absorbance of the $S_2 \leftarrow S_0$ to that of the $S_1 \leftarrow S_0$ transition decreases from 0.9 for Cu^{2+} to 0.15–0.25 for the other ions. Finally, the long wavelength edge of the 0–0 band of the $S_1 \leftarrow S_0$ transition is considerably shallower. Conversely, the features of the fluorescence spectrum of $1-Cu^{2+}$, although bathochromically shifted, resembles quite well those of the other complexes. This makes it unlikely that in $\mathbf{1}-Cu^{2+}$ the nature of the excited state differs strongly from that in the complexes of $\mathbf{1}$ with the other metal ions. In those complexes, the excited state resembles that of a BODIPY fluorophore without strong electron-donating or electron-withdrawing substituents. Taking into account that Cu^{2+} complexes are known to absorb strongly between 550 and 650 nm, the unexpected features of BODIPY in the presence of Cu^{2+} is perhaps attributable to an overlap of the absorption spectrum of BODIPY and that due to dd-transitions of Cu^{2+} in $\mathbf{1}-Cu^{2+}$. The relative short wavelength of the absorption spectrum of Cu^{2+} in $\mathbf{1}-Cu^{2+}$ will lead to a poor overlap with the emission spectrum of $\mathbf{1}-Cu^{2+}$. Hence energy

transfer to the dd-type excited states of Cu^{2+} will be rather slow which may account for the (unexpected) absence of quenching of the BODIPY fluorescence by Cu^{2+} in the $\mathbf{1}$–Cu^{2+} complex.

High selectivity towards the analyte of interest is an important property of any chemosensor. BODIPY indicator $\mathbf{1}$ forms 1:1 complexes with several transition metal (Ni^{2+}, Cu^{2+}, Zn^{2+}) and heavy metal (Cd^{2+}, Hg^{2+}) ions. The dissociation constants K_d of these formed complexes (Table 2) provide numerical criteria for evaluating the selectivity of $\mathbf{1}$ for a particular ion. As shown above, the determination of K_d of each metal ion complex requires the laborious execution and analysis of fluorometric titrations.

In the literature, competitive, steady-state fluorescence measurements are frequently used as a quick alternative for assessing the selectivity of a fluorescent indicator for a certain ion. These simple tests are typically carried out as follows. First, one has to establish through fluorometric titration that the probe is sensitive to a specific ion, let's say X. The analysis of the titration data (eqn 3) yields a value of K_d of the complex with X. To determine if the probe is selective for X, one then measures the steady-state fluorescence signal F_0 (either the whole, integrated fluorescence spectrum or at a single emission wavelength) of the probe in the presence of X at a certain concentration. Subsequently, the competing ion Y at a specific concentration is added to this solution and the fluorescence signal F is measured. The outcome of these competition experiments is often displayed in the form of bar graphs, as presented in Figure S5 (ESI), and shows the change/constancy of the steady-state fluorescence upon addition of the competing ion Y to a solution of the probe in the presence of ion X (X = Cu^{2+} or Cd^{2+} in Figure S5, ESI). If no change is found upon addition of Y, it is commonly assumed that Y does not compete with X

for the probe and hence that the probe is selective for X. We shall show that such fast, easy competition experiments often lead to erroneous conclusions either because the experiments are carried out defectively or for fundamental reasons. For an in-depth investigation of the fluorescence signal F arising from a photophysical system consisting of a probe in the presence of competing ions X and Y, a correct mathematical description of F is needed. Although such analysis is beyond the scope of this paper, it is still possible, without going into mathematical detail, to discuss the present photophysical system (Figure S5, ESI) consisting of **1** in the presence of metal ions X and Y. It can be demonstrated mathematically that the fluorescence F of **1** in the presence of X and Y is dependent on several parameters, namely (i) the K_d values of the complexes of **1** (**1**–X and **1**–Y) with the competing ions X and Y, (ii) the stationary fluorescence F_{min} of the apo form of **1**, (iii) the fluorescence F_{1-X} and F_{1-Y} of the pure complexes **1**–X and **1**–Y, respectively and (iv) the concentrations [X] and [Y] of the unbound (free) ions X and Y, respectively.[28] F describes a 3D data surface as a function of the independent variables [X] and [Y]. Using the equation of F with the above (i–iv) parameters, one can predict mathematically how addition of ion Y to a solution of **1** in the presence of X will affect its steady-state fluorescence F. The dependence of the steady-state fluorescence on the addition of Y at a specific concentration to a solution of **1** in the presence of certain concentration of X is commonly measured by competition experiments (such as those shown in Figure S5, ESI). However, in such experiments only two data points of the full 3D data surface are determined: F_0 and F in Figure S5 (ESI) are even fused into the unique data point F/F_0. F_0 stands for the fluorescence signal of **1** in the presence of 10 μM X (= Cu^{2+} or Cd^{2+}) and F corresponds to **1** in the presence of 10 μM X (= Cu^{2+} or Cd^{2+}) plus a 50 μM solution of other metal ions Y. These two data points and *a priori* the single data

point F/F_0 are insufficient to determine the selectivity of indicator **1** vs. X or Y. Addition of the competitive ion (50 μM) to a solution of **1** in the presence of 10 μM Cu^{2+} (or 10 μM Cd^{2+}) shows no significant variation in the fluorescence intensity. (Figure S5, ESI). This indicates that the fluorescence of **1**–Cu^{2+} (or **1**–Cd^{2+}) is not influenced by other coexisting metal ions Y, at least not at the concentrations used for the original ion X (Cu^{2+} or Cd^{2+}) and the competing metal ions Y.

The near-invariability of the fluorescence intensities F_0 and F (i.e., $F/F_0 \approx 1.0$) cannot be taken as unambiguous proof that **1** is not selective for Y, for the following reasons. It is crucial to start the experiment beginning with the pure complex **1**–X; F_0 should therefore correspond to the fluorescence signal $F_{\mathbf{1}-X}$ of the pure complex **1**–X, which is not the case here. At 10 μM Cu^{2+} (or 10 μM Cd^{2+}) (Figure S5, ESI), the fluorescence intensity of the **1**–Cu^{2+} (or **1**–Cd^{2+}) complex is not reached. This is only the case when the free concentration $[Cu^{2+}]$ (or $[Cd^{2+}]$) is equal to at least $10 \times K_d$ (or preferably $> 10^2 \times K_d$) of the corresponding **1**–Cu^{2+} (or **1**–Cd^{2+}) complex ($K_d = 9$ μM) (see eqn 3).[27] At $[Cu^{2+}]$ (or $[Cd^{2+}]$) = 10 μM and with $K_d = 9$ mM, we are approximately at the mid-point of the titration. Hence, the fluorescent indicator appears both in its free form **1** and its complexed form **1**–X (= **1**–Cu^{2+} or **1**–Cd^{2+}). At low [X] ($[Cu^{2+}]$ or $[Cd^{2+}]$), addition of competing metal ion Y to a mixture containing both **1** and **1**–X (**1**–Cu^{2+} or **1**–Cd^{2+}) may form the complex **1**–Y directly from **1** or/and by displacement of X (Cu^{2+} or Cd^{2+}) from the **1**–X (**1**–Cu^{2+} or **1**–Cd^{2+}) complex. Although under those conditions there might be a change of fluorescence, it is impossible to estimate from these two data points the K_d values of the complex **1**–Y and/or $F_{\mathbf{1}-Y}$. Even if only **1**–X (**1**–Cu^{2+} or **1**–Cd^{2+} in Figure S5, ESI) is present before addition of the competing metal ion Y, constancy of fluorescence upon addition of Y may simply be attributable to the concentration [Y] used that is too low for

influencing the fluorescence. Then, a large excess of [Y] might reveal fluorescence change or invariability in relation to the initial experimental condition where only **1**–X is present. The fluorescence will vary from F_{1-X} (only **1**–X present) at low [Y] ([Y] $\rightarrow$ 0) to F_{1-Y} (only **1**–Y present) for [Y] $\rightarrow$ ∞. However, it is still impossible to estimate a value for K_d of the complex **1**–Y. Theoretically, constancy of the fluorescence as a function of [Y] may also be the result of F_{1-X} and F_{1-Y} being equal ($F_{1-X} = F_{1-Y}$). In this case, the fluorescence remains constant, irrespective of the concentration [Y]. Finally, the competition between X and Y is a dynamic process: it is possible that decomplexation of the original **1**–X complex and/or subsequent formation of the new **1**–Y complex is too slow to occur on the timescale used. To summarize, there are several reasons for the invariability of the fluorescence signal upon addition of Y (too low [Y] used, $F_{1-X} = F_{1-Y}$, decomplexation of **1**–X and/or succeeding formation of **1**–Y is too slow, or the probe is simply not sensitive to Y), so that no reliable decision about the selectivity of the probe can be reached. To conclude, these quick competitive tests are not capable of providing a clear answer to the question of selectivity; only K_d values estimated from fluorometric titrations can do.

Besides selectivity, another important parameter defining fluorescent indicators is sensitivity. Chemosensor **1** forms 1:1 complexes with various transition metal (Ni^{2+}, Cu^{2+}, Zn^{2+}) and heavy metal (Cd^{2+}, Hg^{2+}) ions. An excellent linear correlation (r = 0.994, n = 7) between the steady-state fluorescence F and the Zn^{2+} concentration ($\log[Zn^{2+}]$) was obtained over the range 0–186 μM Zn^{2+} (Figure S6, ESI). The detection limit (DL) was estimated based on the following equation: DL = $3\sigma/k$, where σ is the standard deviation of 10 blank samples (containing only probe **1** without any metal ions) and k is the slope of the calibration curve (fluorescence intensity plotted against [metal ion] or log [metal ion]).[29] The detection limit was

calculated to be as low as 1.0 µM for Zn^{2+}. The sensitivity of the probe towards each metal ion is compiled in Table 3 and is shown to be 1.0 µM or lower.

Table 3. The sensitivity of probe **1** towards each metal ion.

Metal ion	Linear range / µM	F^a	DL / µM	r
Ni^{2+}	0–25.7	$F = 534 - 15.3 \times [Ni^{2+}]$	0.1	0.990
Cu^{2+}	1.5–26	$F = 81.6 + 53.7 \times [Cu^{2+}]$	0.04	0.992
Zn^{2+}	0–186	$F = 5591 + 879 \times \log[Zn^{2+}]$	1.0	0.994
Cd^{2+}	1.3–235.5	$F = 876.7 + 122.2 \times \log[Cd^{2+}]$	0.5	0.994
Hg^{2+}	0–5.3	$F = 389 + 142.7 \times [Hg^{2+}]$	0.01	0.996

[a] Equation used for the fitting of F as a function of ion concentration. The Zn^{2+} and Cd^{2+} concentrations are expressed in M (mol/L), whereas $[Ni^{2+}]$, $[Cu^{2+}]$ and $[Hg^{2+}]$ are in µM.

Conclusions

We have synthesized the visible light excitable, fluorescent BODIPY-based sensor **1**, which shows solvent-dependent spectroscopic/photophysical properties. The generalized treatment of the solvent effect shows that solvent dipolarity is primarily responsible for the observed shifts of the absorption and fluorescence emission maxima. Fluorescent indicator **1** forms 1:1 complexes with several transition metal ions (Ni^{2+}, Cu^{2+}, Zn^{2+}) and heavy metal ions (Cd^{2+}, Hg^{2+}), but not with alkali-metal ions (Na^+, K^+) and earth-alkaline-metal ions (Ca^{2+}, Mg^{2+}). K_d values of the metal ion complexes range from 4 µM for Hg^{2+} to 48 µM for Zn^{2+}. The new compound is an example of a very sensitive fluorescent probe for several metal ions displaying large absorption and fluorescence changes in an analytically interesting wavelength region.

Experimental

The materials used, the steady-state UV–vis absorption and fluorescence spectroscopy, the determination of K_d through direct and ratiometric fluorometric titration are described in the ESI.

Synthesis of 4,4-difluoro-8-(4-methylphenyl)-5-(phenylethynyl)-3-[bis(pyridin-2-ylmethyl)amino]-4-bora-3*a*,4*a*-diaza-*s*-indacene (1). 3-Chloro-4,4-difluoro-8-(4-methylphenyl)-5-(phenylethynyl)-4-bora-3*a*,4*a*-diaza-*s*-indacene (**2**) was synthesized following a literature procedure.[22] To a solution of **2** (104 mg, 0.25 mmol) in acetonitrile (50 mL) under argon atmosphere was added bis(pyridin-2-ylmethyl)amine **3** (60 mg, 0.30 mmol, 1.2 equivs). The reaction mixture was stirred at room temperature for 16 h. Afterwards the resulting solution was poured in water and extracted with dichloromethane (2 × 100 mL). The combined organic layer was washed with brine, dried over $MgSO_4$, filtered and evaporated to dryness under reduced pressure. The crude solid was purified by column chromatography on silica gel using ethyl acetate as eluent to yield 129 mg (89% yield) of a red solid. Mp. 176 °C. ^{1}H NMR ($CDCl_3$) δ 8.55 (d, 2H, J = 4.1 Hz), 7.66 (td, 2H, J = 7.9 Hz, J = 1.5 Hz), 7.48 (dd, 2H, J = 7.9 Hz, J = 1.5 Hz), 7.44 (d, 2H, J = 7.9 Hz), 7.34 (d, 2H, J = 7.9 Hz), 7.28 (m, 3H), 7.24 (d, 2H, J = 7.9 Hz), 7.20 (dd, 2H, J = 5.3 Hz, J = 1.8 Hz), 6.82 (d, 1H, J = 4.9 Hz), 6.59 (d, 1H, J = 4.1 Hz), 6.36 (d, 1H, J = 3.8 Hz), 6.28 (d, 1H, J = 5.2 Hz), 5.29 (s, 4H,), 2.42 (s, 3H, tolyl). ^{13}C NMR ($CDCl_3$) δ 164.2, 156.6, 149.6, 139.2, 137.1, 136.3, 135.4, 133.7, 132.2, 132.0, 131.6, 130.6, 128.2, 128.0, 126.0, 125.6, 123.8, 122.7, 122.1, 120.3, 119.5, 115.3, 100.1, 95.6, 84.0, 58.1, 22.8. IR (cm^{-1}) 3055 (m), 3014 (m), 2920 and 2852 (CH_2, s), 2202 (C≡C, w). LRMS (EI, 70 eV) m/z 579. HRMS: calcd for $C_{36}H_{28}BF_2N_5$ 579.2406, found 579.23967.

^{1}H and ^{13}C NMR spectra were recorded at room temperature on a Bruker 600 instrument operating at a frequency of 600 MHz for ^{1}H and 150 MHz for ^{13}C. ^{1}H NMR spectra were referenced to tetramethylsilane (0.00 ppm) as an internal standard. Chemical shift multiplicities are reported as s = singlet, d = doublet and m = multiplet. ^{13}C spectra were referenced to the $CDCl_3$ (77.67 ppm) signal. Mass spectra were

recorded on a Hewlett Packard 5989A mass spectrometer (EI mode and CI mode). High-resolution mass data were obtained with a KRATOS MS50TC instrument. The IR spectrum was recorded on a Bruker FT-IR spectrometer Alpha-P with Diamond ATR. Melting points were taken on a Reichert Thermovar and are uncorrected.

Electronic Supplementary Information (ESI): Experimental (materials, steady-state UV–vis absorption and fluorescence spectroscopy, determination of K_d through direct and ratiometric fluorometric titration). The Catalán analyses of the solvent-dependent absorption and fluorescence emission maxima. Absorption, fluorescence excitation and emission spectra of **1** in acetonitrile as a function of $[Zn^{2+}]$, $[Cd^{2+}]$ and $[Ni^{2+}]$. Cyclic voltammetry. Fluorescence experiments with competing ions. Sensitivity of **1** towards Zn^{2+}, Cu^{2+} and Ni^{2+}. ^{1}H NMR and ^{13}C NMR spectra of **1** in $CDCl_3$.

References

(1) J.-P. Desvergne and A.W. Czarnik, Eds. *Chemosensors of Ion and Molecule Recognition*; Kluwer: Dordrecht, The Netherlands, 1997.

(2) B. Valeur and J.-C. Brochon, Eds. *New Trends in Fluorescence Spectroscopy. Applications to Chemical and Life Sciences*; Springer: Berlin, 2002.

(3) A. Treibs and F.-H. Kreuzer, *Liebigs Ann. Chem.*, 1968, **718**, 208−223.

(4) (a) A. Loudet and K. Burgess, *Chem. Rev.*, 2007, **107**, 4891-4932; (b) G. Ulrich, R. Ziessel and A. Harriman, *Angew. Chem. Int. Ed.*, 2008, **47**, 1184–1201; (c) N. Boens, V. Leen and W. Dehaen, *Chem. Soc. Rev.*, 2012, **41**, 1130–1172; (d) T. Kowada, H. Maeda and K. Kikuchi, *Chem. Soc. Rev.*, 2015, **44**, 4953–4972; (e) S. Yin, V. Leen, C. Jackers, M. Van der Auweraer , M. Smet, N. Boens and W. Dehaen, *Dyes Pigm.*, 2011, **88**, 372–377; (f) S. Yin, V. Leen, C. Jackers, D. Beljonne, B. Van Averbeke, M. Van der Auweraer , N. Boens and W. Dehaen, *Chem. Eur. J.*, 2011, **17**, 13247–13257.

(5) N. Boens, B. Verbelen and W. Dehaen, *Eur. J. Org. Chem.*, 2015, 6577–6595.

(6) K. Kyose, H. Kojima, Y. Urano and T. Nagano, *J. Am. Chem. Soc.*, 2006, **128**, 6548−6549.

(7) D. W. Gruenwedel*, Inorg. Chem.*, 1968, **7**, 495–501.

(8) G. K. Walkup, S. C. Burdette, S. J. Lippard and R. Y. Tsien, *J. Am. Chem. Soc.*, 2000, **122**, 5644–5645.

(9) (a) K. Kikuchi, K. Komatsu and T. Nagano, *Curr. Opin. Chem. Biol.*, 2004, **8**, 182–191; (b) P. Jiang and Z. Guo, *Coord. Chem. Rev.*, 2004, **248**, 205–229; (c) N. C. Lim, H. C. Freake and C. Brückner, *Chem. Eur. J.*, 2005, **11**, 38–49; (d) P. Carol, S. Sreetjith and S. Ajayaghosh, *Chem. Asian J.*, 2007, **2**, 338–348.

(10) H. Koutaka, J.-i. Kosuge, N. Fukasaku, T. Hirano, K. Kikuchi, Y. Urano, H. Kojima and T. Nagano, *Chem. Pharm. Bull.*, 2004, **52**, 700–703.

(11) Y. Wu, X. Peng, B. Guo, J. Fan, Z. Zhang, J. Wang, A. Cui and Y. Gao, *Org. Biomol. Chem.*, 2005, **3**, 1387−1392.

(12) X. Peng, J. Du, J. Fan, J. Wang, Y. Wu, J. Zhao, S. Sun and T. Xu, *J. Am. Chem. Soc.*, 2007, **129**, 1500−1501.

(13) S. Atilgan, T. Ozdemir and E. U. Akkaya, *Org. Lett.*, 2008, **10**, 4065–4067.

(14) S. C. Dodani, Q. He and C. J. Chang, *J. Am. Chem. Soc.*, 2009, **131**, 18020–18021.

(15) J. A. Cotruvo, Jr., A. T. Aron, K. M. Ramos-Torres and C. J. Chang, *Chem. Soc. Rev.*, 2015, **44**, 4400–4414.

(16) (a) S. Yin, V. Leen, S. Van Snick, N. Boens and W. Dehaen, *Chem. Commun.*, 2010, **46**, 6329–6331; (b) S. Yin, W. Yuan, J. Huang, D. Xie, B. Liu, K. Jiang and H. Qiu, *Spectrochim. Acta A*, 2012, **96**, 82–88; (c) J. Huang, X. Ma, B. Liu, L. Cai, Q. Li, Y. Zhang, K. Jiang and S. Yin, *J. Luminesc.*, 2013, **141**,130–136.

(17) X. Jia, X. Yu, G. Zhang, W. Liu and W. Qin, *J. Coord. Chem.*, 2013, **66**, 662–670.

(18) X. Yu, X. Jia, X. Yang, W. Liu and W. Qin, *RSC Adv.*, 2014, **4**, 23571–23579.

(19) E. M. Nolan and S. J. Lippard, *Chem. Rev.*, 2008, **108**, 3443–3480.

(20) H. N. Kim, W. X. Ren, J. S. Kim and Y. Yoon, *Chem. Soc. Rev.*, 2012, **41**, 3210–3244.

(21) W. Qin, T. Rohand, W. Dehaen, J. N. Clifford, K. Driessen, D. Beljonne, B. Van Averbeke, M. Van der Auweraer and N. Boens, *J. Phys. Chem. A*, 2007, **111**, 8588 – 8597.

(22) T. Rohand, W. Qin, N. Boens and W. Dehaen, *Eur. J. Org. Chem.*, 2006, 4658−4663.

(23) J. Catalán, *J. Phys. Chem. B*, 2009, **113**, 5951–5960.

(24) L. Jiao, C. Yu, J. Wang, E. A. Briggs, N. A. Besley, D. Robinson, M. J. Ruedas-Rama, A. Orte, L. Crovetto, □E. M. Talavera, J. M. Alvarez-Pez, M. Van der Auweraer and N. Boens, RSC Adv., 2015, 5, 89375- 89388.

(25) (a) W. Qin, M. Baruah, M. Sliwa, M. Van der Auweraer, D. Beljonne, B. Van Averbeke, N. Boens, *J. Phys. Chem. A*, 2008, **112**, 6104–6114; (b) W. Qin, V. Leen, T. Rohand, W. Dehaen, P. Dedecker, M. Van der Auweraer, K. Robeyns, L. Van Meervelt, D. Beljonne, B. Van Averbeke, J. N. Clifford, K. Driesen, K. Binnemans and N. Boens, *J. Phys. Chem. A*, 2009, **113**, 439–447; (c) I. Esnal, J. Bañuelos, I. López Arbeloa, A. Costela, I. Garcia-Moreno, M. Garzón, A. R. Agarrabeitia and M. J. Ortiz, *RSC Adv.*, 2013, **3**, 1547–1556.

(26) E. Cielen, A. Tahri, A. Ver Heyen, G. J. Hoornaert, F. C. De Schryver and N. Boens, *J. Chem. Soc., Perkin Trans. 2*, 1998, 1573−1580.

(27) A. Kowalczyk, N. Boens, V. Van den Bergh and F.C. De Schryver, *J. Phys. Chem.*, 1994, **98**, 8585−8590.

(28) N. Boens, unpublished results.

(29) W. Qin, W. Liu and M. Tan. *Anal. Chim. Acta*. 2002, **468**, 287–292.

Supporting Information

A ratiometric, fluorescent BODIPY-based probe for transition and heavy metal ions

Wenwu Qin,[#,*] **Wei Dou,**[#] **Volker Leen,**[†] **Wim Dehaen,**[†] **Mark Van der Auweraer**[†] **and Noël Boens**[†,*]

[#] *Key Laboratory of Nonferrous Metal Chemistry and Resources Utilization of Gansu Province and State Key Laboratory of Applied Organic Chemistry, College of Chemistry and Chemical Engineering, Lanzhou University, Lanzhou 730000, China*

[†] *Department of Chemistry, KU Leuven (Katholieke Universiteit Leuven), Celestijnenlaan 200f, 3001 Leuven, Belgium*

Contents

[*] Corresponding authors: E-mail: qinww@lzu.edu.cn (W. Qin) and Noel.Boens@chem.kuleuven.be (N. Boens)

Experimental

Materials

All solvents for the spectroscopic measurements were of spectroscopic grade and were used without further purification. Metal perchlorates of the highest purity available were purchased from Beijing J & K Chemical Technology Co (Beijing, China) and were dried in a vacuum oven before use. The chemicals for the synthesis were of reagent grade quality, procured from commercial sources, and used as received.

Steady-state UV–vis absorption and fluorescence spectroscopy

Dilute solutions of **1** in different solvents were prepared by dissolving the dry, powered dye in the appropriate solvent so that the absorbance at the maximum of the main absorption peak was $\leq$ 0.1 using 1-cm optical path length (corresponding to a dye concentration in the μM range). UV–vis absorption spectra were recorded on a Varian UV-Cary100 spectrophotometer, and for the corrected steady-state excitation and emission spectra, a Hitachi F-4500 spectrofluorometer or an Edinburgh Instruments FLS920 was employed. Freshly prepared samples in 1-cm quartz cells were used to perform all UV–vis absorption and emission measurements. For the determination of the fluorescence quantum yields Φ of **1**, only dilute solutions with an absorbance below 0.1 at the excitation wavelength (λ_{ex} = 530 nm, except for DMF, CH$_3$CN and DMSO with λ_{ex} = 510 nm) were used. Cresyl violet in methanol (Φ_r = 0.55) was used as fluorescence reference.[1] The Φ values reported in Table 1 are the averages of three fully independent measurements. The standard uncertainties on the Φ values were 0.01–0.02. In all cases, correction for the solvent refractive index was applied. All spectra were recorded at 20 °C using nondegassed samples.

Determination of K_d through *direct* fluorometric titration

The ground-state dissociation constants K_d of the complexes between **1** and various cations were determined in CH$_3$CN solution at 20 °C by *direct* fluorometric titration as a function of the cation concentration [X] using the fluorescence excitation or emission spectra. Nonlinear fitting of eqn 3 to the steady-state fluorescence data F recorded as a function of [X] yields values of K_d, F_{min}, F_{max} and n.[2]

Determination of K_d through *ratiometric* fluorometric titration

If spectral shifts are observed in the excitation and/or emission spectra upon binding of the cation X by the probe, then *ratiometric* fluorometric titrations as a function of the cation concentration [X] – using ratios of the fluorescence excitation or emission spectral data – can be used to determine K_d and n of the probe–cation complex. This is the case for **1** and various cations. Nonlinear fitting of eqn 4 to the steady-state fluorescence ratios R recorded as a function of [X] yields values of $K_d\xi$, R_{min}, R_{max} and n.[2]

Solvent dependence of absorption and fluorescence emission maxima

The solvent effect on the physicochemical observable y is described by the multilinear expression 1:

$$y = y_0 + a_{SA}\, SA + b_{SB}\, SB + c_{SP}\, SP + d_{SdP}\, SdP \tag{1}$$

where y_0 denotes the physicochemical property of interest in the gas phase; a_{SA}, b_{SB}, c_{SP} and d_{SdP} are adjustable coefficients that reflect the dependency of the physicochemical property y in a given solvent on the {SA, SB, SP, SdP} solvent parameters. SA, SB, SP and SdP are four mutually independent, empirical solvent scales – introduced by Catalan[3] – that characterize respectively the <u>s</u>olvent <u>a</u>cidity, <u>b</u>asicity, <u>p</u>olarizability and <u>di</u>polarity. The physicochemical characteristics y analyzed are the absorption maxima $\bar{\nu}_{abs}$ [$= 1/\lambda_{abs}(max)$] and the fluorescence emission maxima $\bar{\nu}_{em}$ [$= 1/\lambda_{em}(max)$], both expressed in cm^{-1}. The {SA, SB, SP, SdP} parameters for an extensive list of solvents can be found in ref. 3.

The advantage of the generalized (i.e., Catalán) treatment of the solvent effect over all the other approaches is that it allows one to disentangle the relative contributions of dipolarity, polarizability, acidity and basicity of the medium. Hence, it is instructive to determine by the Catalán methodology which solvent properties contribute primarily to the observed solvatochromic shifts of $\bar{\nu}_{abs}$ and $\bar{\nu}_{em}$.

The fit of $\bar{\nu}_{abs}$ of **1** according to eqn 1 with {SA, SB, SP, SdP} as independent variables yields a large d_{SdP} estimate with high precision (i.e., comparatively small standard error) in relation to {a_{SA}, b_{SB}, c_{SP}} with relatively high standard errors (Table S1). This is indicative that the change of $\bar{\nu}_{abs}$ reflects predominantly a change in dipolarity of the environment of the dye. The large positive d_{SdP}-value is in agreement with the fact that more (di)polar solvents (increasing SdP) produce a hypsochromic shift of $\lambda_{abs}(max)$ (i.e., larger $\bar{\nu}_{abs}$). This suggests a decreased dipole moment of **1** in S_1 compared to S_0. If SdP was left out as independent variable in the analyses of $\bar{\nu}_{abs}$ of **1** according to eqn 1 (that is, with {SA, SB, SP}), a low r-value (0.172) was found, implying the importance of this solvent parameter. Conversely, the three analyses of $\bar{\nu}_{abs}$ according to eqn 1, in which the common independent variable is SdP (i.e., with {SA, SB, SdP}, {SB, SP, SdP} and {SA, SP, SdP} as independent variables), all gave high-quality fits (with r = 0.935, 0.883 and 0.939, respectively). Further corroboration for SdP as major factor comes from the six analyses with two solvent scales as independent variables: the three analyses with SdP (i.e., with {SA, SdP}, {SB, SdP} and {SP, SdP}) all gave high r-values (> 0.862), whereas the three other analyses (without SdP) yielded unacceptable fits (r < 0.171). The crucial role of solvent dipolarity was finally confirmed by the high-quality linear relationship (r = 0.860) between $y = \bar{\nu}_{abs}$ and SdP and the inadequate linear fits of $y = \bar{\nu}_{abs}$ as a function of SA, SB and SP, respectively (r = 0.137, 0.017 and 0.065, respectively). Additional evidence that solvent polarizability does not influence the position of $\bar{\nu}_{abs}$ can be inferred from the unacceptable fit of $y = \bar{\nu}_{abs}$ vs. $f(n)$ $= (n^2 - 1)/(2n^2 + 1)$ (r = 0.271).

The Catalán {SA, SB, SP, SdP} solvent scales (eqn 1) also describe adequately the solvatochromic shifts of $\bar{\nu}_{em}$ ($r = 0.827$, Table S1). To find out which solvent properties predominantly account for the shifts of $\bar{\nu}_{em}$, we performed some additional regression analyses according to eqn 1 in which systematically one, two and three solvent scales were omitted. These analogous analyses of $\bar{\nu}_{em}$ of **1** indicated that dipolarity is the main factor determining the position of $\bar{\nu}_{em}$. For example, the analyses in which one solvent scale was omitted clearly identify solvent dipolarity as the most critical one for $\bar{\nu}_{em}$. Indeed, the three analyses of $\bar{\nu}_{em}$ according to eqn 1, in which SdP is the common independent variable, all gave fits with r between 0.803 and 0.825. In contrast, the analysis of $\bar{\nu}_{em}$ according to eqn 1, in which solvent dipolarity was left out, produced a much lower low r-value (0.218). Hence, as found for $\bar{\nu}_{abs}$, solvent dipolarity is the most important solvent property determining the position of $\bar{\nu}_{em}$ and this is confirmed by the linear regression of $y = \bar{\nu}_{em}$ vs. SdP ($r = 0.790$). Extra corroboration that solvent polarizability does not determine the position of $\bar{\nu}_{em}$ can be inferred from the unacceptable fit of $y = \bar{\nu}_{em}$ vs. $f(n) = (n^2 - 1)/(2n^2 + 1)$ ($r = 0.415$).

Table S1. Estimated coefficients (y_0, a_{SA}, b_{SB}, c_{SP}, d_{SdP}; eqn 1), their standard errors and correlation coefficients (r) for the multilinear regression analyses of $\bar{\nu}_{abs}$ and $\bar{\nu}_{em}$ of **1** for the solvents listed in Table 1 as a function of the Catalán solvent scales. The estimates are expressed in cm^{-1}.

|	y_0	a_{SA}	b_{SB}	c_{SP}	d_{SdP}	r
$\bar{\nu}_{abs}$	$(18.2 \pm 0.5) \times 10^3$	-841 ± 249	-54 ± 170	-625 ± 649	$(1.3 \pm 0.1) \times 10^3$	0.939
$\bar{\nu}_{abs}$	$(17.8 \pm 0.6) \times 10^3$		-305 ± 201	71 ± 812	$(1.2 \pm 0.2) \times 10^3$	0.883
$\bar{\nu}_{abs}$	$(18.1 \pm 0.4) \times 10^3$	-876 ± 217		-610 ± 626	$(1.3 \pm 0.1) \times 10^3$	0.939
$\bar{\nu}_{abs}$	$(17.7 \pm 0.1) \times 10^3$	-765 ± 236	-42 ± 169		$(1.3 \pm 0.1) \times 10^3$	0.935
$\bar{\nu}_{abs}$	$(18.3 \pm 0.1) \times 10^3$	-401 ± 677	183 ± 464	137 ± 1780		0.172
$\bar{\nu}_{em}$	$(17.2 \pm 0.3) \times 10^3$	-178 ± 142	31 ± 97	-474 ± 371	392 ± 77	0.827
$\bar{\nu}_{em}$	$(17.1 \pm 0.3) \times 10^3$		-22 ± 89	-327 ± 359	374 ± 77	0.804
$\bar{\nu}_{em}$	$(17.2 \pm 0.3) \times 10^3$	-158 ± 124		-483 ± 358	395 ± 73	0.825
$\bar{\nu}_{em}$	$(168.5 \pm 0.6) \times 10^2$	-120 ± 138	41 ± 99		380 ± 78	0.803
$\bar{\nu}_{em}$	$(17.2 \pm 0.4) \times 10^3$	-45 ± 234	103 ± 161	-244 ± 616		0.218

Binding of transition metal and heavy metal ions by 1
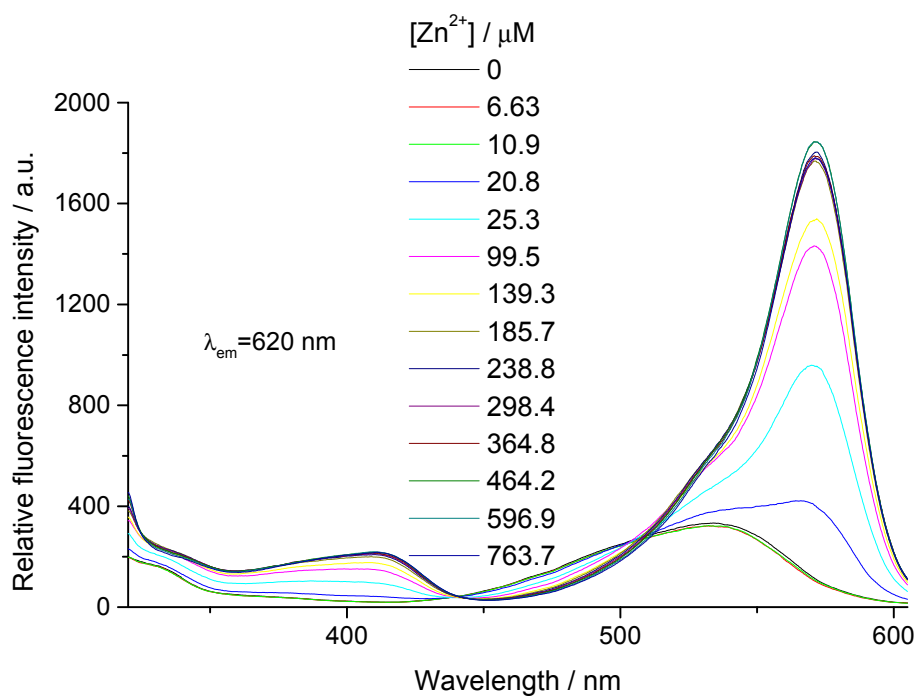
Figure S1. Fluorescence excitation spectra of compound **1** in acetonitrile solution as a function of $[Zn^{2+}]$ (emission observed at 620 nm).
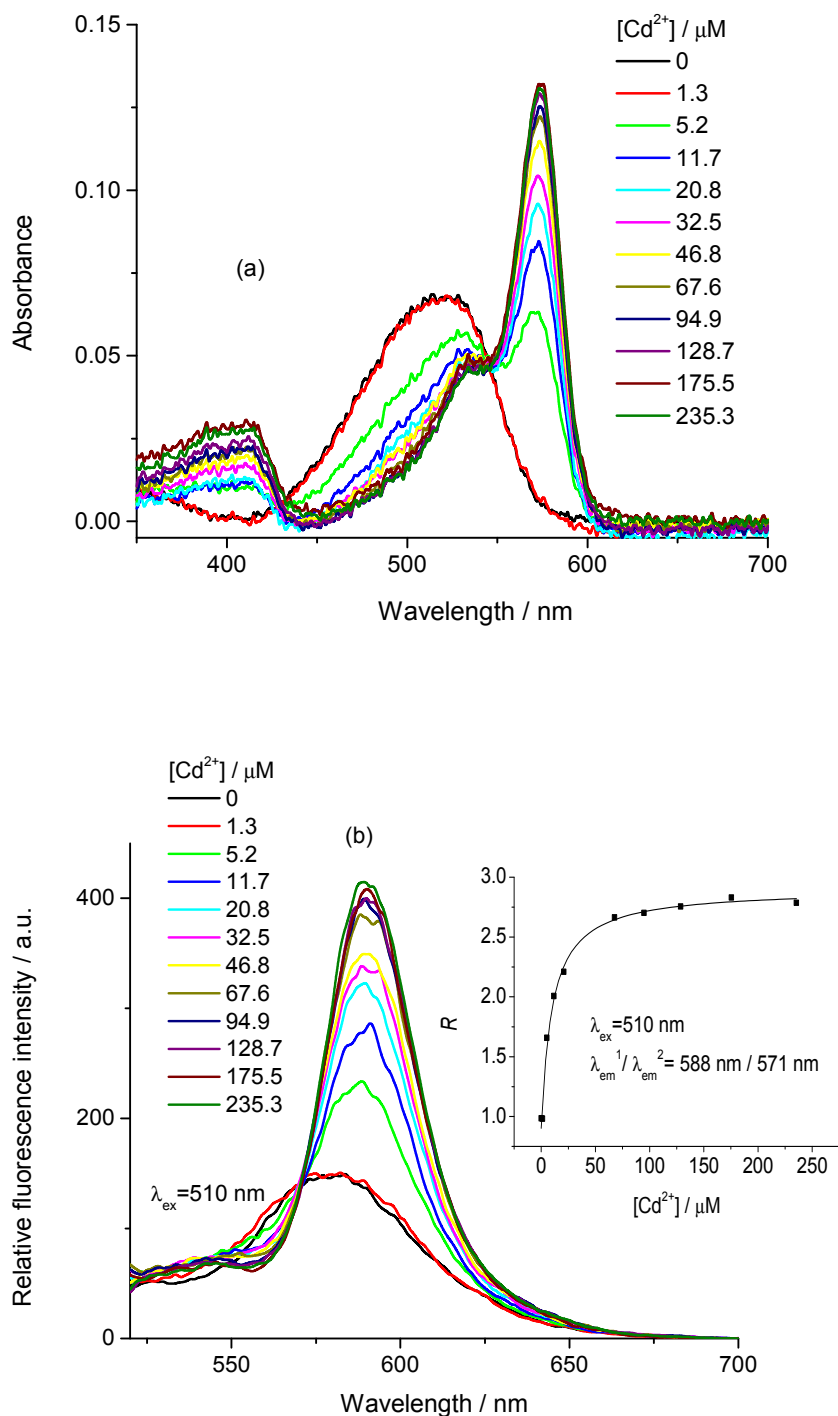
**Figure S2.** Compound **1** in acetonitrile solution as a function of $[Cd^{2+}]$. (a) Absorption spectra. (b) Fluorescence emission spectra (excitation at 510 nm). The full line in the inset of (b) shows the best fit to the ratiometric emission titration data (eqn 4 with $n = 1$) at $\lambda_{em}^1/\lambda_{em}^2 = 588$ nm/571 nm (isoemissive point) as a function of $[Cd^{2+}]$.
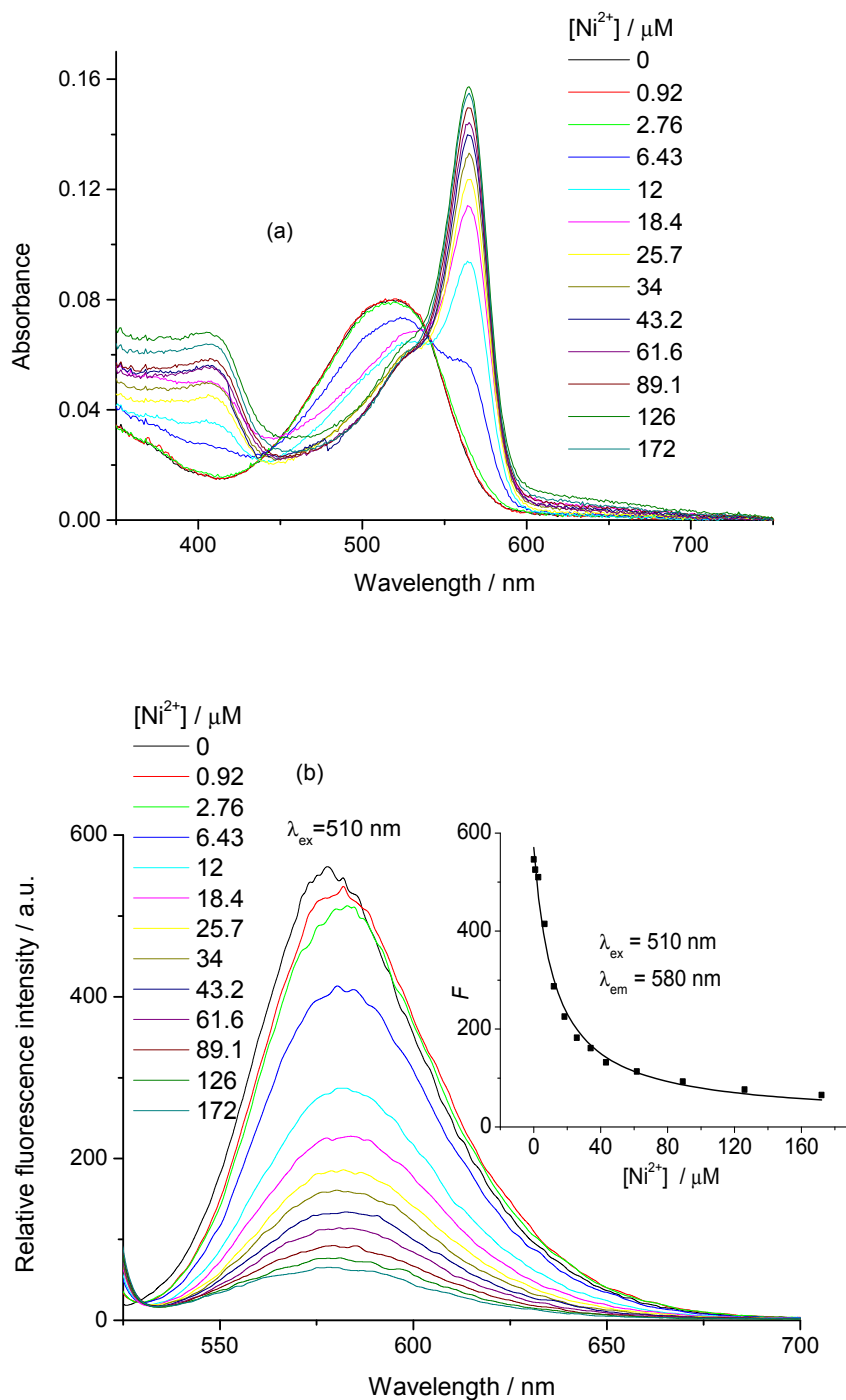
Figure S3. Compound **1** in acetonitrile solution as a function of [Ni^{2+}]. (a) Absorption spectra. (b) Fluorescence emission spectra (excitation at 510 nm). The full line in the inset of (b) shows the best fit to the direct fluorometric emission (eqn 3 with n = 1) titration data at λ_{em} = 580 nm as a function of [Ni^{2+}].

Electrochemistry

Electrochemical data were obtained using a CHI600B potentiostat and a standard three-electrode cell [platinum working and platinum counter electrodes, and a Hg/saturated calomel electrode (SCE) reference] at a scan rate of 100 mV s^{-1}. The voltammograms were recorded at room temperature using a solution of 0.1 mol/L tetrabutylammonium hexafluorophosphate as the supporting electrolyte in dry dichloromethane. All solutions were purged with argon prior to measurement. Figure S4 displays the cyclic voltammogram for **1** showing the one-electron oxidations. The oxidation potentials E_{ox} of **1** estimated from the midpoints of the forward and reverse peaks of the scan appear at ca. +0.82 and +0.97 V vs. SCE, respectively. These values are close to, but somewhat lower than that of the symmetric BODIPY derivative with phenylethynyl groups at the 3,5-positions (E_{ox} = +1.02 V).[4] This indicates that a DPA group is slightly more electron-donating than the phenylethynyl moiety. Substitution of the inductively electron-withdrawing chlorine atom for the DPA subunit in **1** renders oxidation of the chlorine-containing compound more difficult (E_{ox} = +1.52 V).[4] We did not observe any reduction electrochemistry and this may be because these redox potentials are beyond the accessible range of dichloromethane.
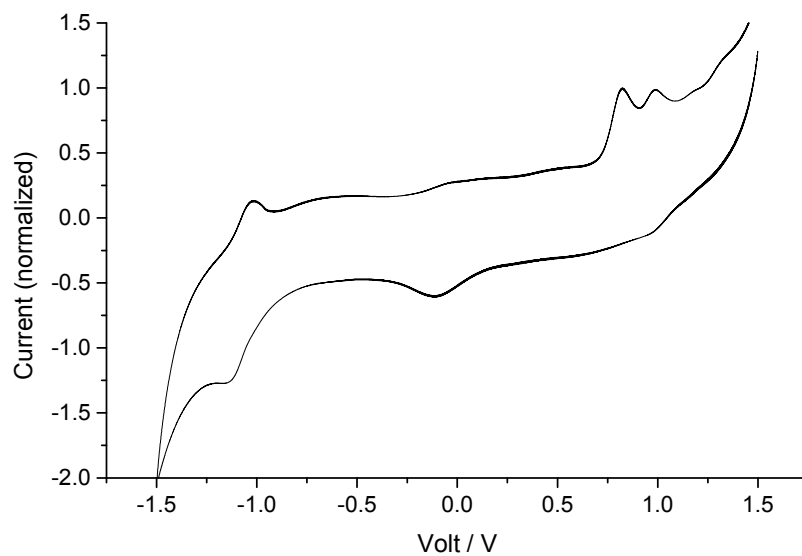
Figure S4. Cyclic voltammogram of **1** in degassed dichloromethane solution containing 0.1 mol L^{-1} tetrabutylammonium hexafluorophosphate using a scan rate of 100 mV s^{-1}. The potentials are expressed vs. a Hg/saturated calomel electrode reference.

Competition experiments

(a)

(b)
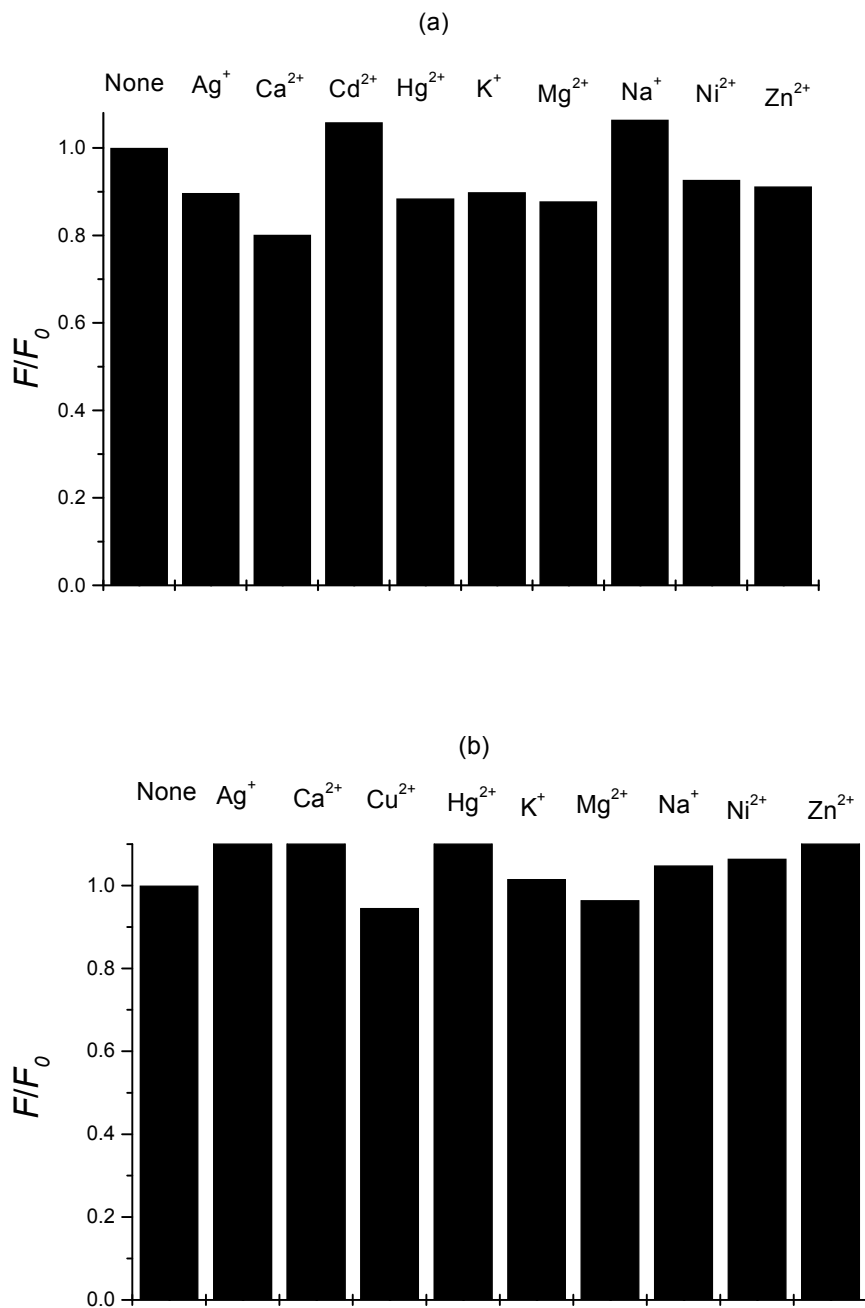
Figure S5. The bars show the fluorescence emission change that occurs to a solution of **1** in the presence of (a) 10 μM Cu^{2+} or (b) 10 μM Cd^{2+} in acetonitrile upon injection of a 50 μM acetonitrile solution of other competing metal ions. The competing ion is indicated on top of each bar. F_0 and F represent the whole, integrated emission spectrum of **1** in the presence of (a) 10 μM Cu^{2+} or (b) 10 μM Cd^{2+}. F_0 is measured in the absence of competing ions, whereas F is obtained in the presence of 50 μM competing ion.

Relationship between *F* and ion concentration
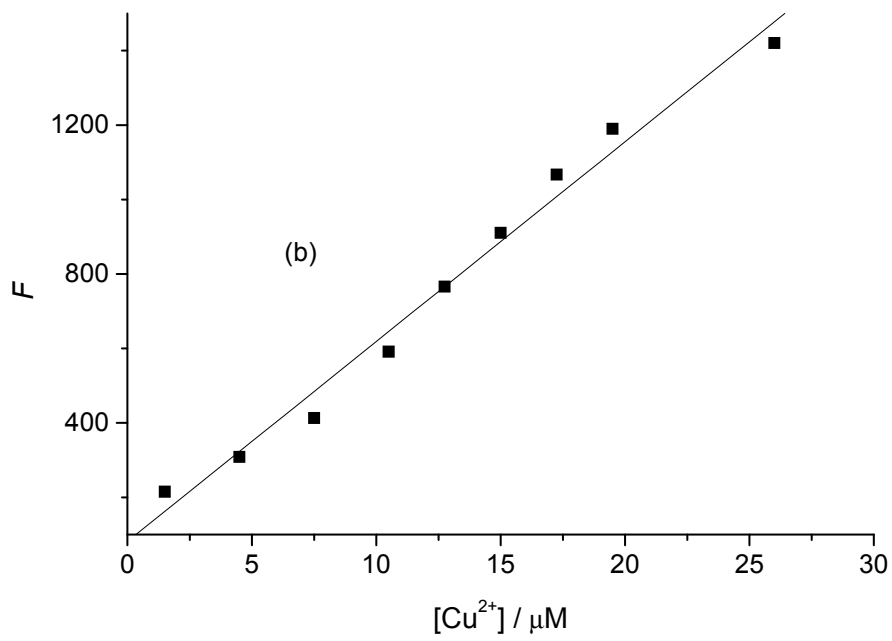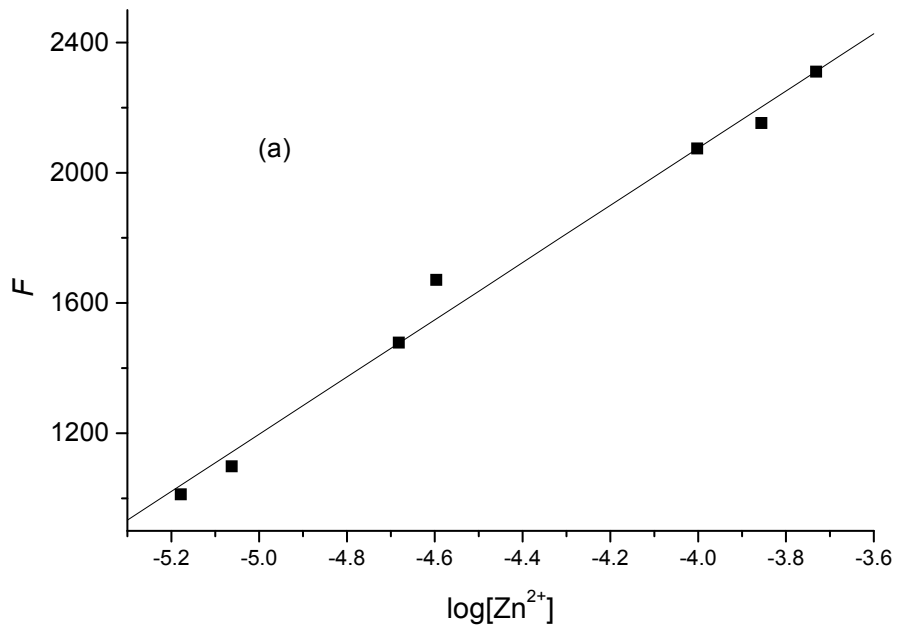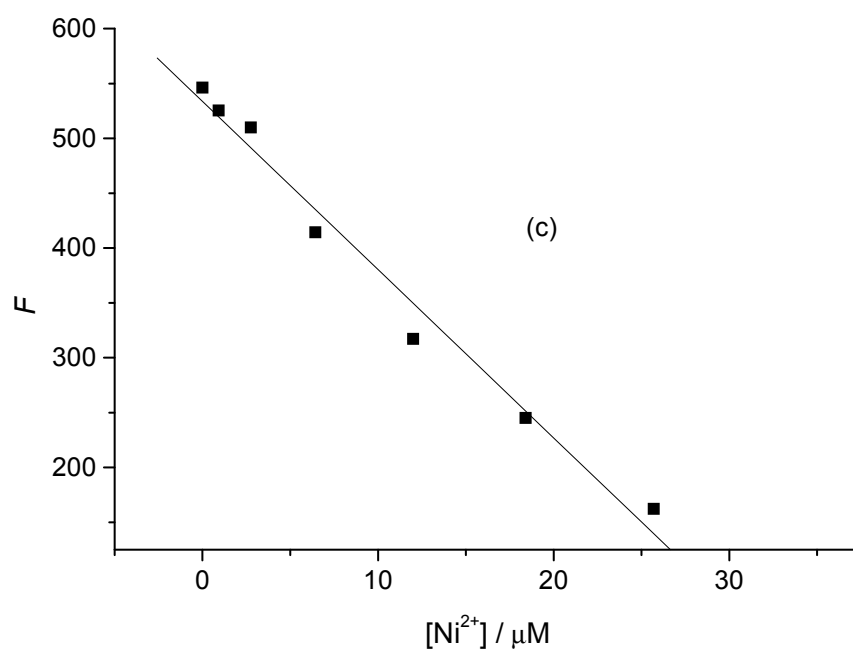
Figure S6. (a) Fluorescence emission F measured at 584 nm (λ_{ex} = 510 nm) for **1** in acetonitrile solution as a function of log[Zn^{2+}] ([Zn^{2+}] = 0–280 μM, data obtained from part of the spectra of Figure 3b). (b) Linear relationship between F at 616 nm (λ_{ex} = 510 nm) and [Cu^{2+}] ([Cu^{2+}] = 0–25.7 μM, data obtained from part of the spectra of Figure S3b). (c) Linear relationship between F at 580 nm (λ_{ex} = 510 nm) and [Ni^{2+}] ([Ni^{2+}] = 0–25.7 μM, data obtained from part of the spectra of Figure 5b).

NMR spectra of 1
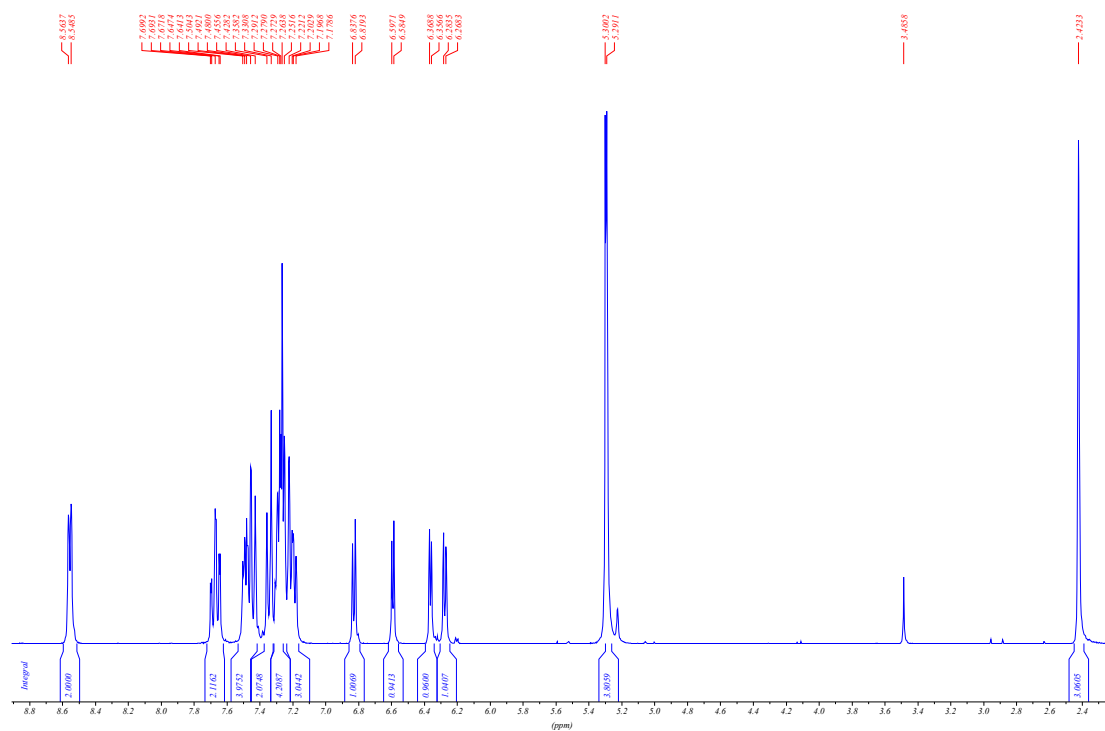
^{1}H NMR of **1** in CDCl$_3$ ↑
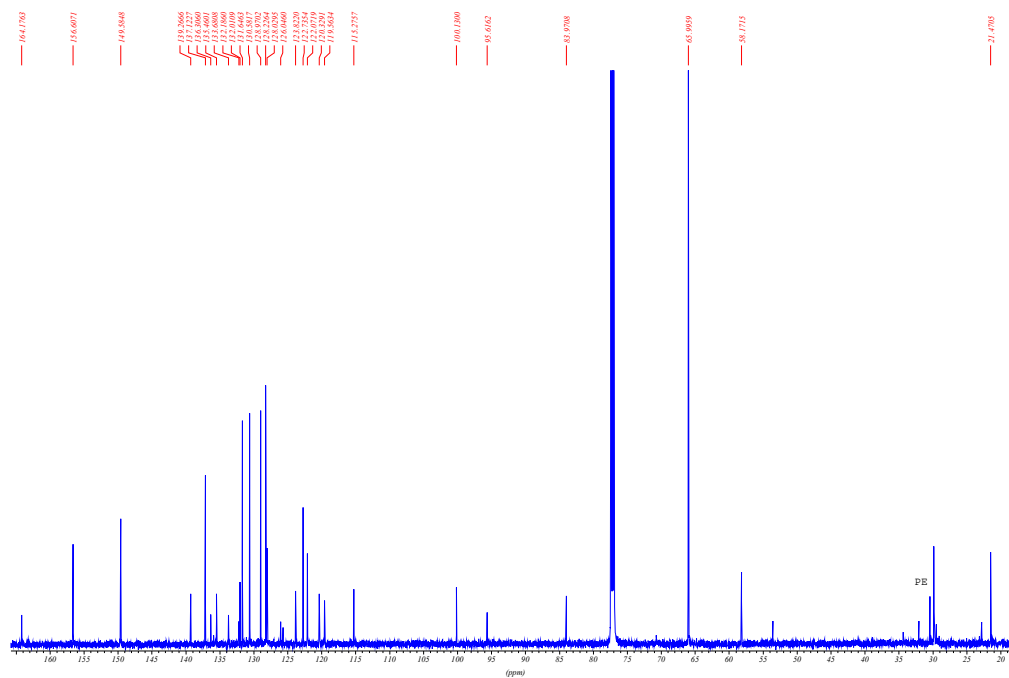
^{13}C NMR of **1** in CDCl$_3$ ↑

References

(1) J. Olmsted, *J. Phys. Chem.*, 1979, **83**, 2581−2584.

(2) E. Cielen, A.. Tahri, A. Ver Heyen, G. J. Hoornaert, F. C. De Schryver and N. Boens, *J. Chem. Soc.*, *Perkin Trans. 2*, 1998, 1573−1580.

(3) J. Catalán, *J. Phys. Chem. B*, 2009, **113**, 5951–5960.

(4) W. Qin, T. Rohand, W. Dehaen, J. N. Clifford, K. Driessen, D. Beljonne, B. Van Averbeke, M. Van der Auweraer and N. Boens, *J. Phys. Chem. A*, 2007, **111**, 8588−8597.